D.F. McDonough, J.A. Taylor, A.D. Pillsbury,
D.P. Verly, E.S. Kintzer, and J.G. Garcia

A Space-Qualified Transmitter System for Heterodyne Optical Communications

A space-based optical communications system requires the development of high-precision yet rugged electro-optical hardware. As part of a program to develop this technology, Lincoln Laboratory has designed and constructed a laser transmitter and a companion diagnostics module that have passed a rigorous space-qualification test program. The transmitter and diagnostics module are critical components of a satellite-to-satellite, 220 Mb/sec heterodyne communications experiment. The transmitter includes four redundant 30-mW diode lasers in a compact, lightweight package. The diagnostics module enables precise and autonomous setting of the transmitter laser power, wavelength, and modulation characteristics. The successful qualification of these components is a first, and a major milestone in the development of spaceborne optical communications systems.

For nearly three decades, researchers have tried to develop an optical system for communications in space [1–3]. Although the gas lasers used in early projects were successful in laboratory demonstrations, the bulk and fragility of these laser systems made them unsuitable for space applications. Recently, however, the evolution of small, robust, and highly efficient semiconductor diode lasers has rekindled hopes for space-qualified optical communications systems [4–6].

Optical communications systems would offer a number of benefits over conventional radio-frequency systems for certain space applications [7]. Such systems could allow space communications at very high data rates with smaller and lighter packages. Such communications is possible because optical systems operating at short wavelengths can produce very narrow beams with modest-sized telescopes and because optical systems can have large communications bandwidths. The narrow beams also enable communications that is resistant to jamming and interception. In addition to increasing the capacity and security of certain military communications, high-data-rate, narrow-beam optical communications links could be important for deep-space exploration and research.

Optical communications systems, however, require tremendous precision. The narrow beamwidths require highly accurate pointing so that the laser power can be concentrated on the distant receiver. Limited laser power dictates that beam aberrations and attenuation must be carefully controlled. Typically, unacceptable power losses can be caused by aberrations resulting from submicron-level movement of critical optical elements. Therefore, the development of optical communications hardware for space requires careful and thorough design, assembly, and testing.

This article will describe the successful development and flight qualification testing of two critical units of a diode-laser-based transmitter system for heterodyne space communications. The two units—a transmitter assembly and a companion diagnostics module—form part of a complete engineering model of a space package. The transmitter and diagnostics module, both designed and developed by Lincoln Laboratory, are key components of a realizable optical system for heterodyne space communications.

Laser Intersatellite Transmission Experiment

Project Description

The transmitter system is part of Lincoln Laboratory's Laser Intersatellite Transmission

Acronyms

ACTS	Advanced Communications Technology Satellite
CPM	Coarse-Pointing Mirror
FEM	finite-element model
FPI	Fabry-Perot interferometer
FSK	frequency-shift keying
FWHM	full width at half-maximum
LITE	Laser Intersatellite Transmission Experiment
LO	local oscillator
OMS	Optomechanical Subsystem
SNR	signal-to-noise ratio
SSM	Source Select Mechanism
TLC	Transmitter Laser Controller

Experiment (LITE) (see the box, "Acronyms"), which is developing critical technology for satellite-to-satellite communications. On the basis of proven laboratory hardware, Lincoln Laboratory is building and qualifying rugged, compact modules suitable for space applications to provide crosslink capabilities at up to 220 Mb/sec over synchronous-orbit distances. By doing so, we expect to reduce the technological risk in future flight programs.

The LITE flight package was designed to fly on the NASA Advanced Communications Technology Satellite (ACTS). (Note: LITE is no longer part of the ACTS program; substitute host spacecraft are being investigated.) The package would be placed in a geosynchronous orbit in which the spacecraft would be attitude stabilized in pitch and roll to an angular accuracy of about 1 mrad. Thus the ACTS project dictated the launch and orbit conditions for the LITE program (Table 1). The qualification tests reported in this article are designed to meet those requirements, and are conservative enough to include possible levels of most, if not all, spacecraft.

The LITE flight package consists of two major modules designed for mounting at separate locations within the host spacecraft:

1. the Optomechanical Subsystem (OMS) [8], which contains all of the optical elements

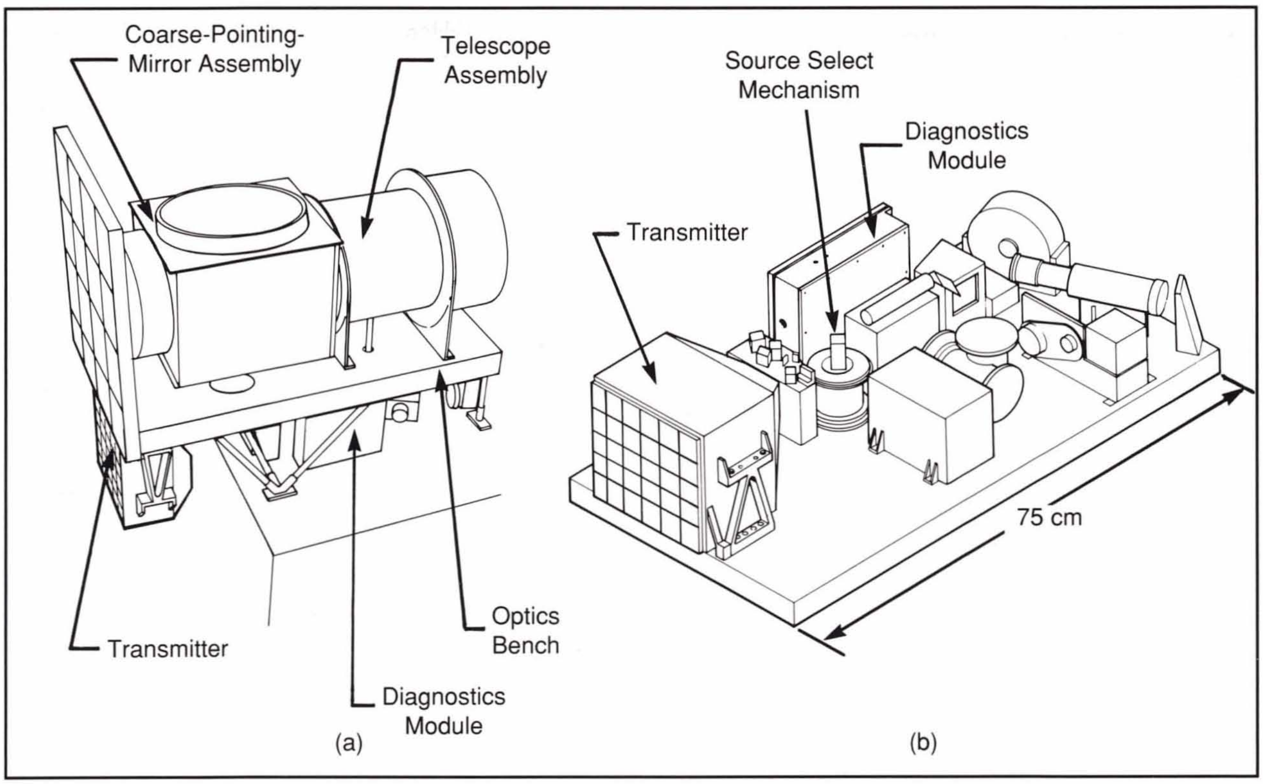

Fig. 1—LITE Optomechanical Subsystem: (a) top (earth-facing) view showing the telescope and pointing mirror, and (b) bottom view showing the transmitter, diagnostics module, beam steering and tracking optics, and relay optics. The supporting truss is not shown in part b.

Table 1. Key Launch and Orbit Conditions for the Laser Intersatellite Transmission Experiment (LITE) Flight Package

Exposure	*Level*	*Duration*
Launch/deployment temperature extremes	–40° to 60°C	Cycling
Operational temperature extremes	–5° to 50°C	Cycling
Random vibration		
Optomechanical Subsystem	6.5 g (rms)	1 min
Electronics Module	12.9 g (rms)	1 min
Acoustic noise	140 dB	1 min
Static loading	20.7 g	Maximum condition

of the system, a small amount of local electronics, and the necessary supporting structure; and

2. the Electronics Module, which contains those electronic circuits which can be remotely located within the spacecraft structure.

The OMS, designed to be located on the earth-facing panel of the ACTS spacecraft, includes a benchlike structure supported by a truss network that provides thermal and vibrational isolation from the host vehicle. On the top (earth-facing) side of the bench (Fig. 1[a]) are a 20-cm-diameter Dall-Kirkham telescope and a steerable mirror called the Coarse-Pointing Mirror (CPM). After receiving a beacon beam from the receiver's platform, the telescope transmits a diffraction-limited beam of 4-μrad divergence. The CPM allows the transmitted beam to be directed to any geosynchronous or low-earth-orbit receiver above the horizon. On the bottom side of the OMS bench (Fig. 1[b]) are the transmitter, the diagnostics module, the fine beam steering and tracking optics, and the associated relay optics.

LITE was designed for intersatellite communications. However, initial transmission tests would send data through the atmosphere to a ground station at a good astronomical site.

Overview of Transmitter System

The LITE transmitter system, with components in both the OMS and Electronics Module (Fig. 2), consists of the transmitter itself and the associated modules that control the laser operating parameters. Table 2 lists the transmitter system's key characteristics. From the Electronics Module, the transmitter receives electrical power, laser bias current, temperature-control power, command signals, and data-modulation signals. The transmitter's beam is directed to either the telescope or the diagnostics module by the two-axis Source Select Mechanism (SSM), which operates under closed-loop control to stabilize the beam.

The LITE system uses heterodyne detection with 4-ary frequency-shift-keyed (FSK) modulation at rates up to 220 Mb/sec. In 4-ary FSK, the optical frequency is shifted between four possible values, or tones (Fig. 3). The LITE system uses tones that are spaced at 220-MHz intervals, and the system performs heterodyne detection by mixing the received beam with the output from a local-oscillator (LO) laser that operates at nearly the same optical frequency as the received beam [2]. To extract the data stream, the system processes the resulting beat frequency as an RF signal. Because the beat frequency must be stable to within several megahertz, a frequency-acquisition and tracking loop is required to control the LO laser. For the frequency-acquisition loop to function, the beat frequency must fall within the receiver's 1-GHz passband. This requirement makes it necessary for the receiver to know, *a priori*, the initial transmitted frequency with an accuracy significantly better than 1 GHz out of an operating frequency greater than 10^{14} Hz. In addition, the alignment of the

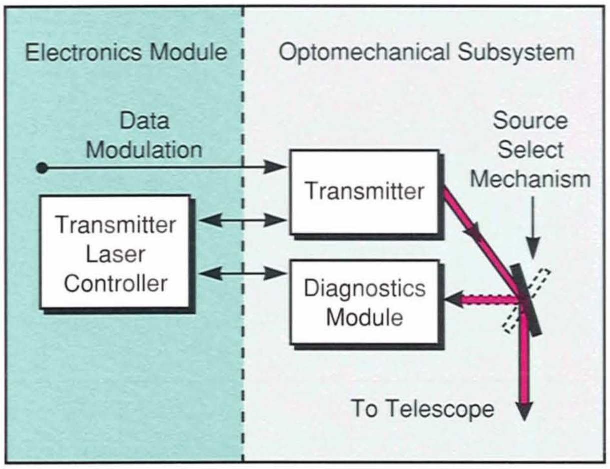

Fig. 2—Block diagram of the Laser Intersatellite Transmission Experiment (LITE) transmitter system.

transmitted FSK tone to the receiver's filter passbands requires a tone spacing of 220 MHz ±5 MHz to keep energy losses to less than 0.1 dB (Fig. 4).

The LITE transmitter uses four redundant GaAlAs diode lasers (Fig. 5), each of which emits a nominal 30-mW beam in a single spatial mode at a single frequency. The operating frequency of the diode lasers depends very strongly on the operating temperature (30 GHz/°C) and bias current (3 GHz/mA). Consequently, to maintain the desired frequency stability the transmitter system must set and hold the operating temperature with a precision better than 0.001°C and the bias current with a precision better than 10 μA. In addition, the laser-power output must be kept to 30 mW ± 1 mW. Higher powers reduce the laser lifetime; lower powers reduce the communications performance.

To satisfy all of these requirements, LITE incorporates an autonomous diagnostics system that measures and sets the laser wavelength, power, and FSK tone spacing. At the beginning of a communications session, the transmitted beam is directed to the diagnostics module. A microprocessor-based controller, the Transmitter Laser Controller (TLC), monitors the diagnostics-module signals to measure and set the transmitter's operating parameters.

The task of setting the laser's operating point is complicated by the laser tuning characteristics illustrated in Fig. 6. Using a two-step process to avoid tuning through discontinuities (laser mode hops), the TLC sets the laser optical frequency to within 100 MHz (or wavelength to within 0.0025 Å) of an atomic reference.

The next two sections describe the transmitter and diagnostics system in greater detail.

Transmitter Description

Features

The performance of the transmitter is critical to successful communications. The transmit-

Table 2. Transmitter System Characteristics

Transmitter mass	1.96 kg (4.3 lbs)
Diagnostics-module mass	1.26 kg (2.8 lbs)
Transmitter electrical power	<4.2 W (during communications)
Diagnostics-module electrical power	1.1 W
Laser wavelength	0.86 μm
Number of lasers	4 (1 active, 3 spares)
Wavefront quality	λ/20 (rms), λ = wavelength
Beam profile	Circular, Gaussian, 5-mm diameter
Optical power (incl. losses)	26 mW ± 1 mW
Optical-frequency accuracy	100 MHz
FSK tone spacing	220 MHz ± 5 MHz
Laser-modulation bandwidth	1 GHz

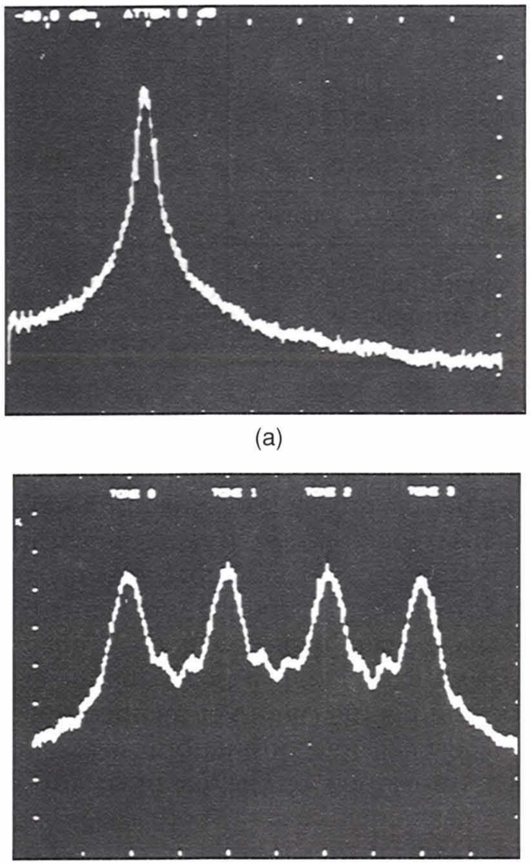

(a)

(b)

Fig. 3—Intermediate-frequency spectra: (a) unmodulated and (b) with 4-ary frequency-shift keying (FSK) of pseudorandom bit stream. The horizontal scale is 100 MHz/division and the vertical scale is 5 dB/division.

ter's output beam must remain highly collimated and precisely pointed, in spite of the vibration and temperature variations of launch and orbit. The LITE communications power budget requires that the beam's phase profile be flat to within $\lambda/20$ (rms) where λ is the wavelength, that its pointing be centered on the SSM to within 100 μm, and that optical power losses be kept to less than 0.8 dB. A precise, thorough optomechanical design is required to achieve these goals.

Each laser's initial operating temperature will be at a specific temperature between 15° and 25°C to achieve the desired wavelength. Furthermore, a laser's operating temperature may change with age. For these reasons, the transmitter is designed to operate from 10° to 30°C. Careful attention to thermal design and control and an athermal focus design are vital.

The transmitter design, shown schematically in Fig. 7, is based on four modular units known as source assemblies (Fig. 8), each with a diode laser that can be frequency modulated via the injection current for data rates up to 220 Mb/sec. Each source assembly contains a lens assembly that collimates the highly divergent output of the laser into a beam of elliptical cross section. A foil heater located behind the laser mounting plate and a feedback thermistor located next to the laser maintain temperature control of the laser. A small printed circuit board in the source assembly combines the DC bias and modulation signal. The board also contains a circuit for selecting which laser is active.

Although there are four lasers in the transmitter, only one is operated at any given time. The remaining lasers are backups that are included because the long-term reliability of the selected lasers has not been fully proven yet.

We have found several advantages to making source-assembly modules interchangeable. This approach allows (1) the critical collimation procedure and testing to be performed outside of

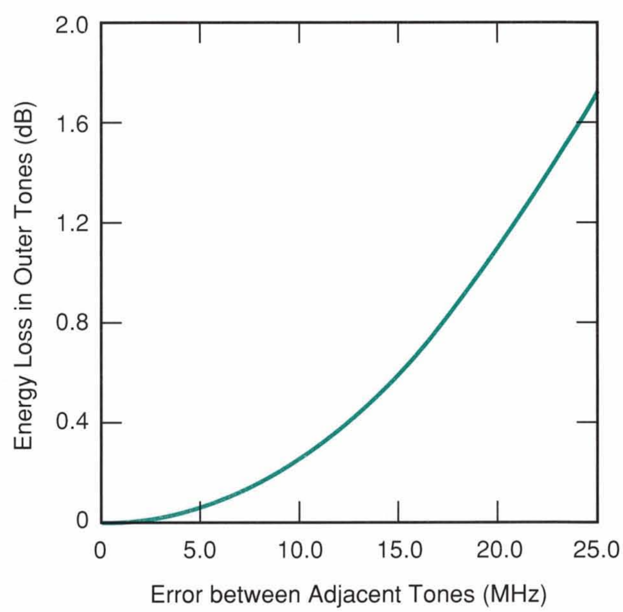

Fig. 4—The theoretical energy loss in the outer FSK tones versus the tone-spacing error. (The effective energy loss in the FSK demodulation would be slightly less.) Note that the loss approaches 0.1 dB at a 5-MHz error.

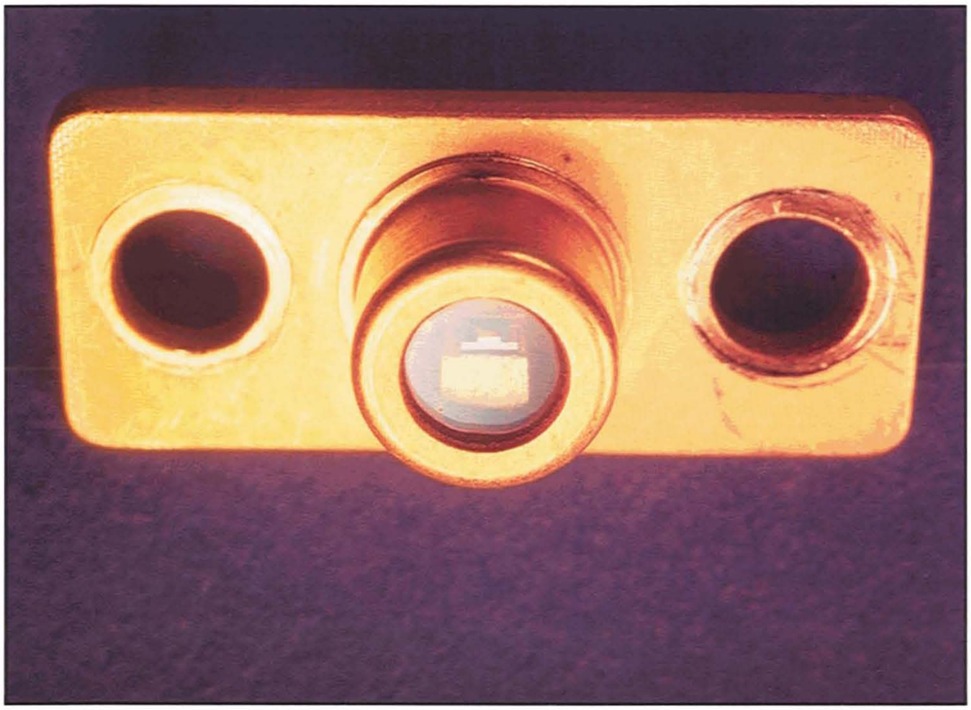

(a)

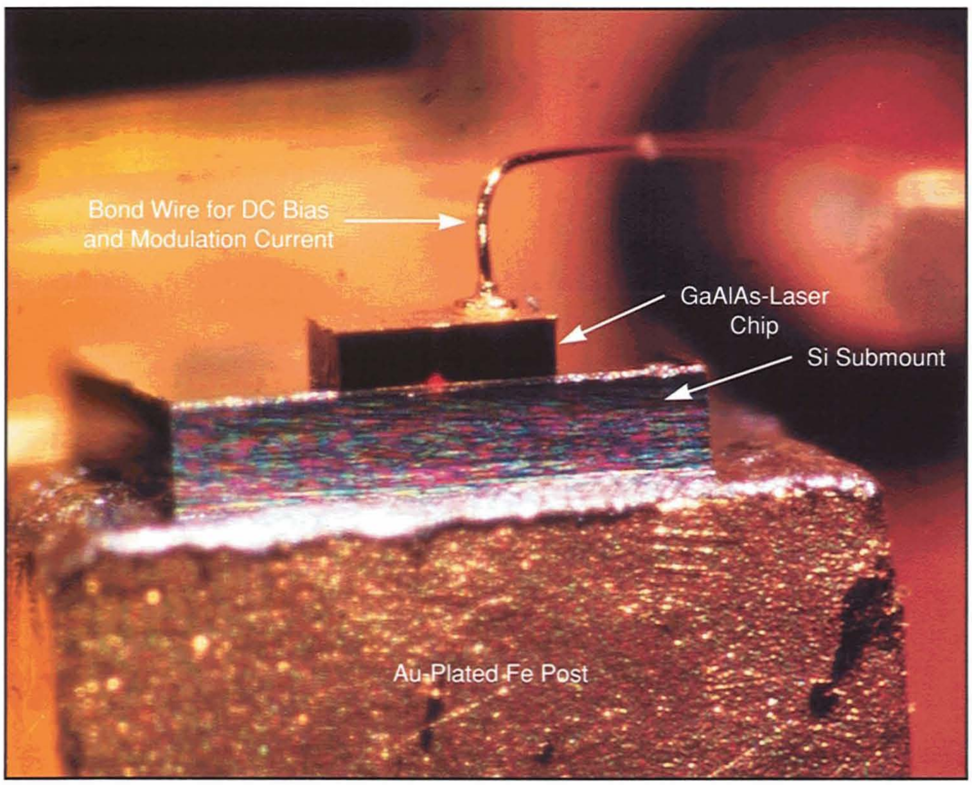

(b)

Fig. 5—Diode laser used in LITE: (a) packaged laser 16 mm × 7 mm and (b) microphotograph of laser.

the limited confines of the transmitter, (2) the lasers to be exchanged readily when necessary, and (3) the source assembly to be used by itself in other applications such as in the receiver's local oscillator.

The selected laser—a Hitachi channeled-substrate planar device—was the highest-power single-mode diode laser meeting our requirements that was commercially available when the LITE project commenced. We selected the laser's center wavelength in the vicinity of 0.86 μm to coincide with a transmission window in the atmosphere for initial space-to-ground testing of the LITE system. We then selected specific operating wavelengths to match the absolute

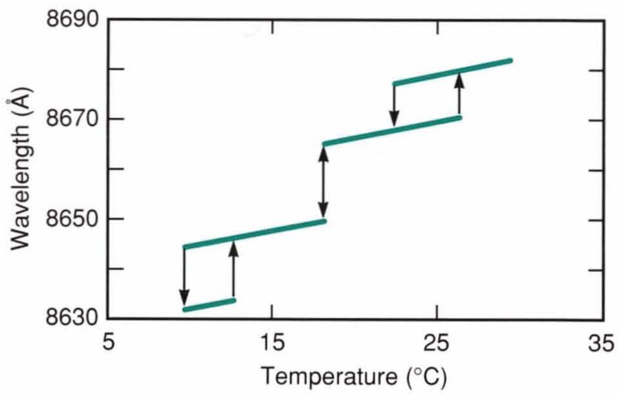

Fig. 6—Typical laser tuning curve. Note that the tuning regions are discontinuous and that about 25% of the overall wavelength range is accessible. The tuning regions typically span 3 to 6 Å.

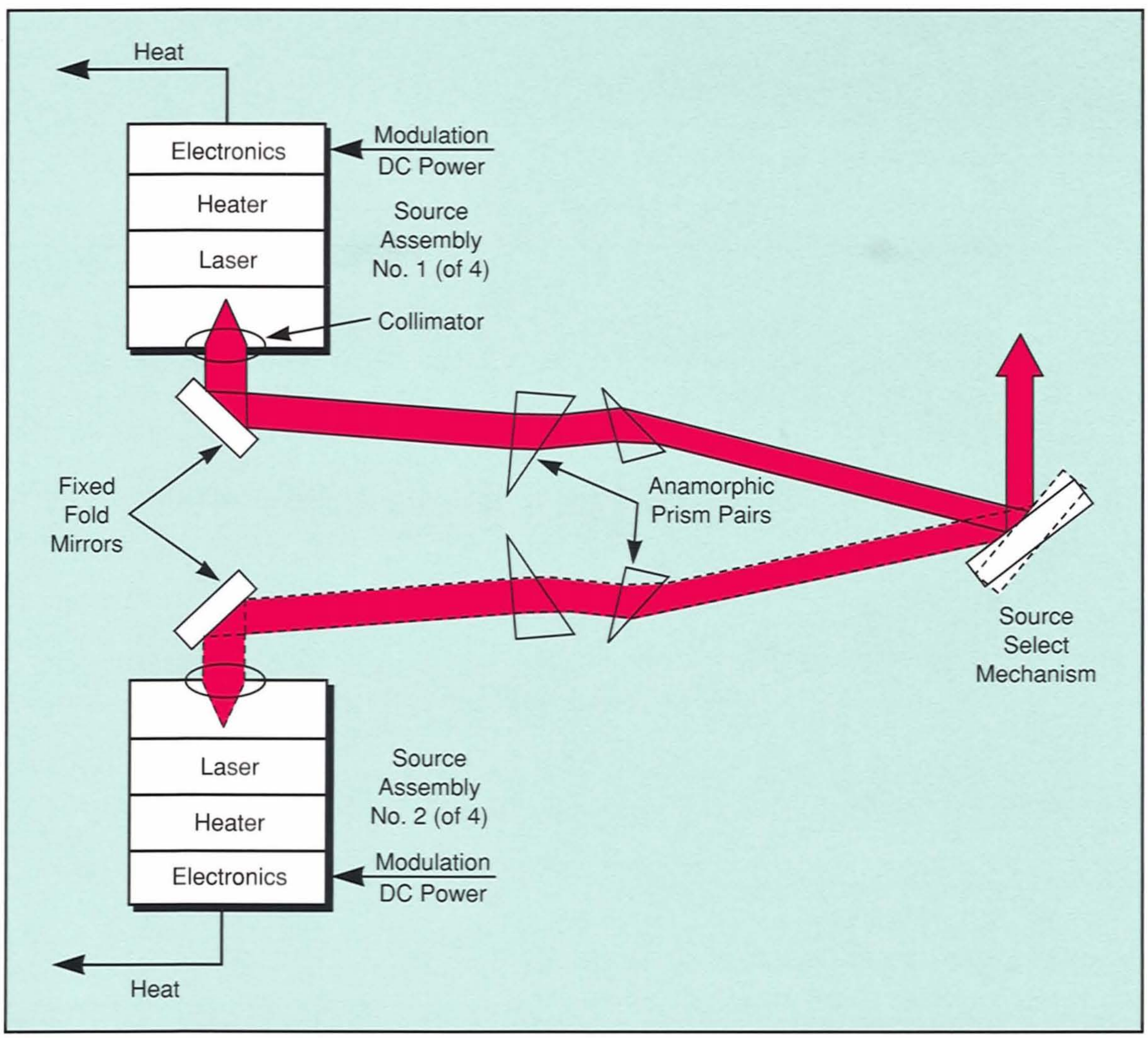

Fig. 7—Schematic of LITE transmitter.

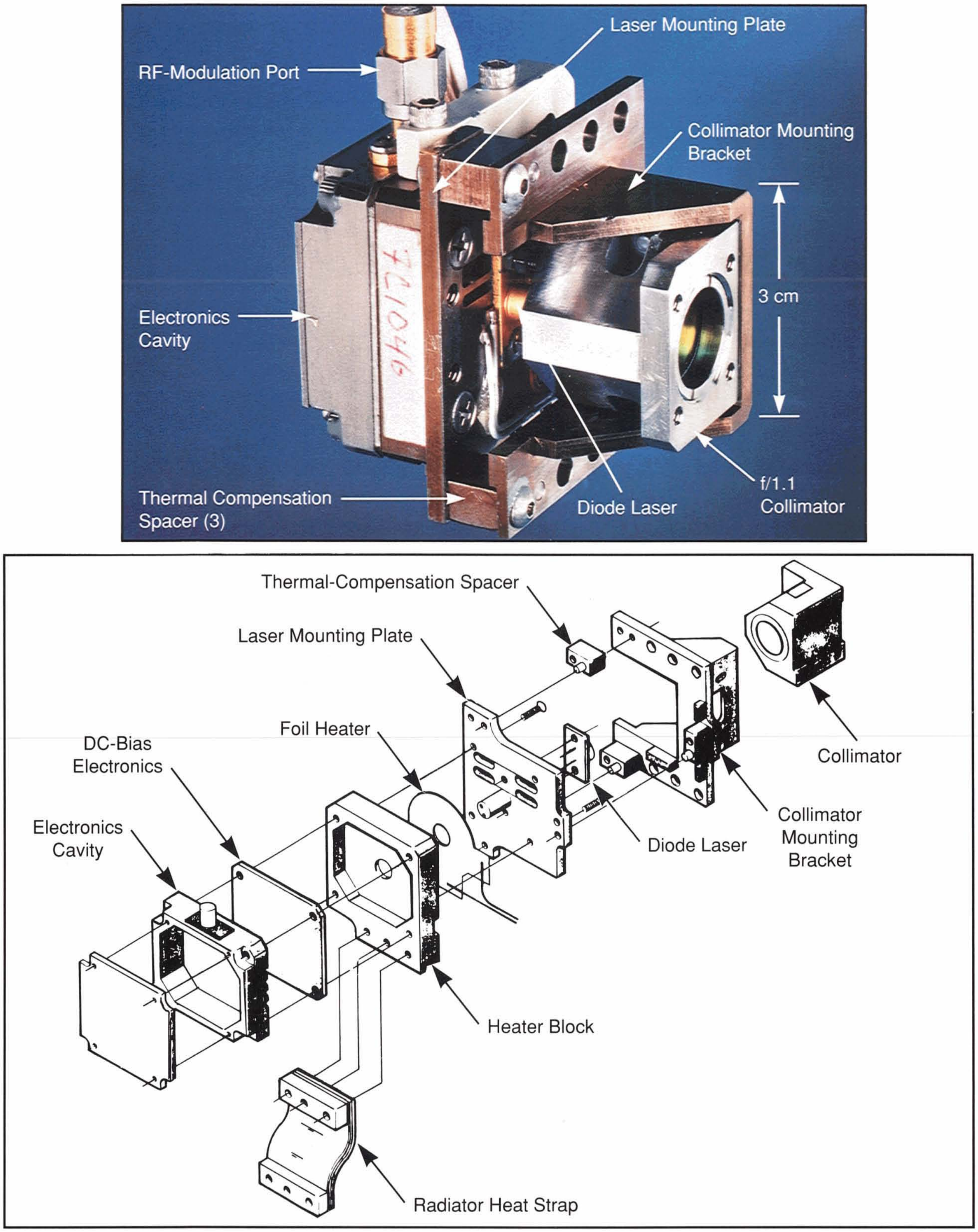

Fig. 8—Source assembly, which contains a diode laser, collimating lens assembly, part of a temperature control circuit, and a small printed circuit board. The source assembly has a mass of 160 g and an RF-modulation bandwidth of approximately 1 GHz.

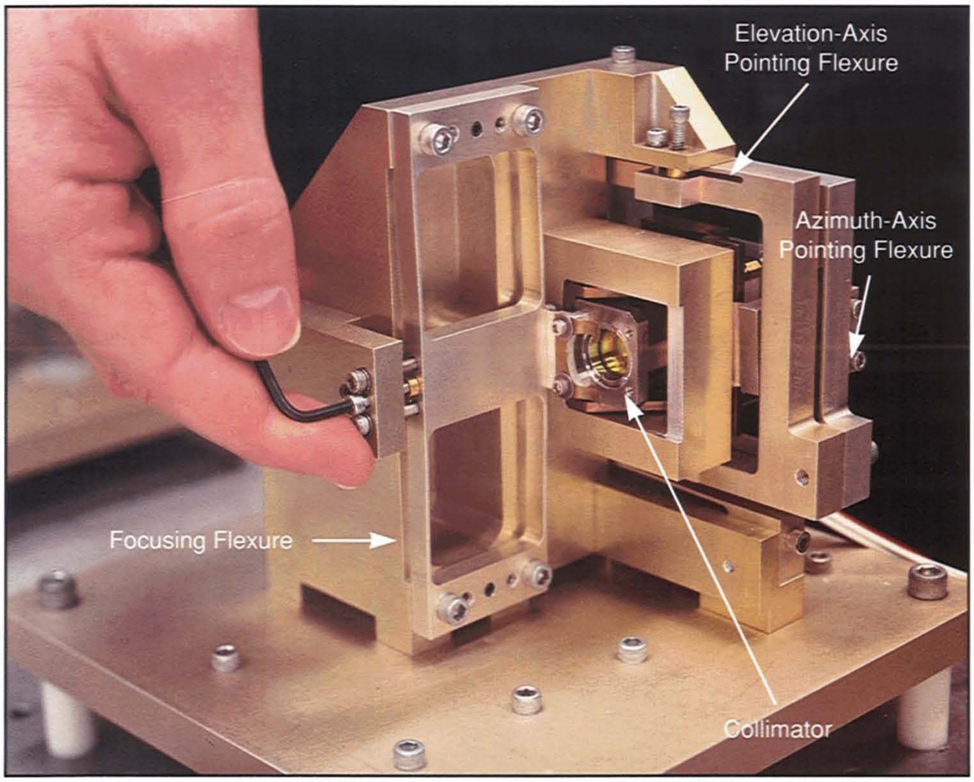

Fig. 9—Source-assembly alignment stand for positioning and securing the collimator with respect to the diode laser. To achieve high wavefront quality and beam-pointing accuracy, the push-pull flexures allow submicron positioning accuracy in three axes.

wavelength standard of the atomic transitions of neon, which is used as a reference in the diagnostics module.

The lasers were rigorously screened and tested before incorporation into the transmitter. These tests included operation at an elevated temperature for 80 hours, full characterization, continuous operation for an additional 170 hours, and recharacterization. The screening and testing process identified the most stable lasers with the best optical characteristics. For the class of laser selected, we expect lifetimes of 10^4 to 10^5 hours.

To achieve the necessary high wavefront quality, not only must the collimator be carefully designed and fabricated, it must also be fixed at the correct position with respect to the diode laser. Our most difficult challenge in the assembly of the sources was to keep the collimator in precise focus while we secured its position. We developed techniques to achieve and maintain a positional accuracy of 0.5 μm with the alignment fixture shown in Fig. 9.

All of the transmitter components are supported by a titanium structure [9, 10] (Figs. 10 and 11). The four source assemblies are mounted on the top and bottom surfaces of the support structure with each of the collimated output beams aimed vertically to a dedicated fold mirror that directs the beam to an anamorphic prism pair. This prism pair compresses the elliptical beam into a circular, 5-mm-diameter beam. We arranged the prisms so that the four output beams intersect at the SSM mirror's center of rotation.

Heating of the transmitter is provided by foil heaters, and passive cooling is provided by a radiator, which faces deep space. The radiator is supported by the transmitter frame and is attached to the source assemblies via flexible straps.

In order to limit the truncation loss in the telescope to an acceptable level, translations of the beam at the SSM must be small. We calculated that a 100-μm translation at the SSM would yield a tolerable loss of 0.11 dB. Thus we took great care in implementing the optomechanical design because beam pointing is a function of several factors—the position of the laser with respect to the collimator, the source-assembly position with respect to the transmitter, the anamorphic-prism positions, and any deformations of the support structure.

As discussed previously, the requirements for the thermal design are stringent. The temperature of the OMS bench below the transmitter can be as much as 30°C colder than the source assemblies. For this reason, careful attention was paid to providing adequate thermal isolation between the OMS and the transmitter:

- The three support struts are made of titanium (a material with low thermal conductivity) with a small cross-sectional area.
- The wiring harness has a small number of wires of the smallest practical gauge.
- The jacket of the coaxial modulation cable is made from low-thermal-conductivity stainless steel.
- A lightweight cover, which is not shown in Figs. 10 or 11, encloses the transmitter to provide protection against contamination and to support a multilayer thermal insulation blanket that minimizes radiative coupling.

The completed transmitter has a mass of 1.96 kg, only a small percentage of the overall mass of the LITE package, and is expected to consume less than 4.2 W during operation in space, including the heater power.

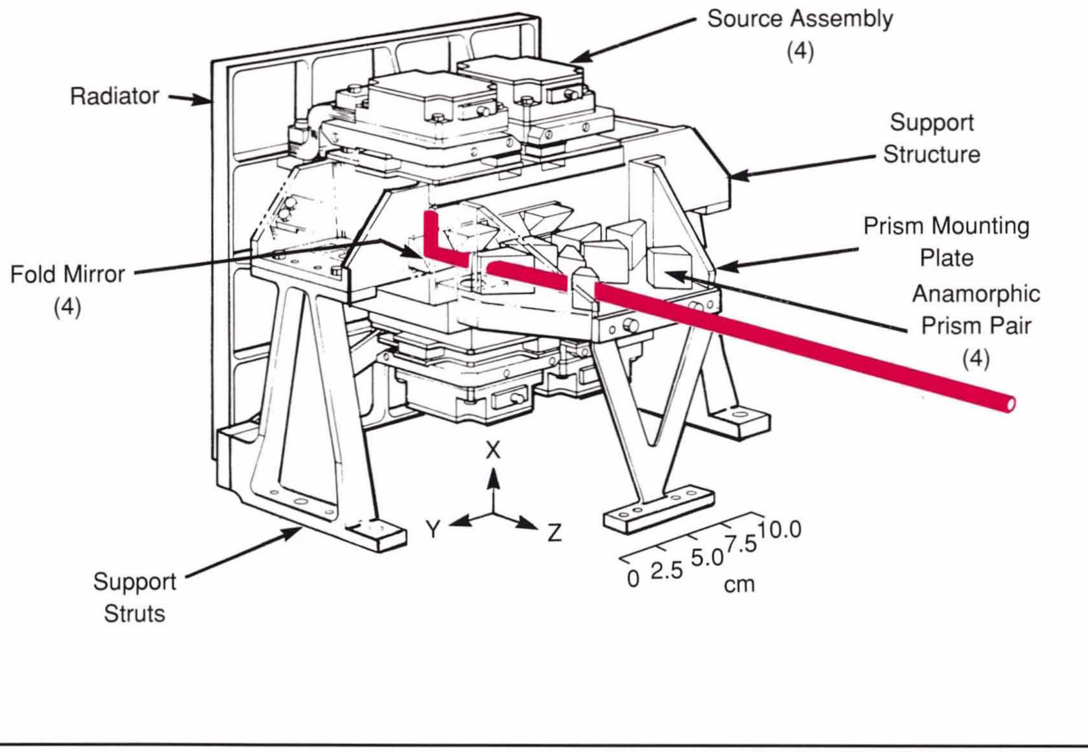

Fig. 10—The transmitter contains four source assemblies, each of which produces a high-quality collimated beam of elliptical cross section. Pairs of prisms are used to circularize the beams. A thermal radiator is attached to the source assemblies by means of flexible thermal straps to eliminate waste heat.

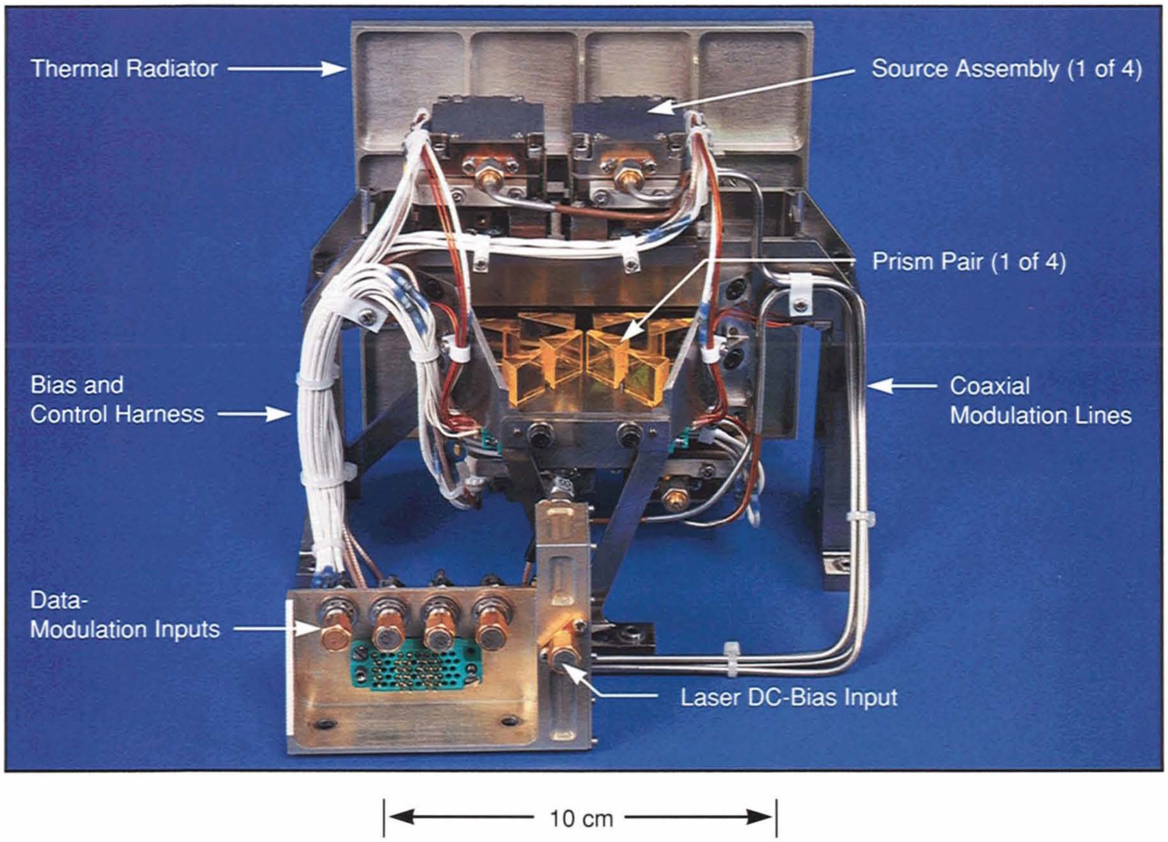

Fig. 11—Qualification transmitter, which has a mass of 1.96 kg and consumes less than 5 W. The transmitter maintained good beam quality and pointing after being subjected to repeated thermal cycling from –30 to 66°C and random vibration at up to 16.2 g (rms).

Design Analysis

After we had established the general features of the transmitter, we proposed a candidate design and subjected it to extensive computer analysis. The analysis was necessary to determine whether we could expect the proposed transmitter to survive launch and operate satisfactorily in the space environment.

Prediction of the transmitter performance required the interaction of three separate computer models: a finite-element model (FEM), a thermal model, and a ray-tracing optical analysis program. The FEM estimated the structural distortions and stresses due to dynamic and static loads from both launch and operating disturbances. The FEM also calculated the thermally induced distortions and stresses by using the results from the separate thermal model, which determined the temperature distributions within the transmitter for various scenarios. The thermal model included the effects of solar illumination on the radiator face, conductive and radiative coupling with the OMS, and power dissipation within the transmitter's heaters and circuit boards. Finally, the ray-tracing optical analysis program generated the optical sensitivities for motions of all elements along the optical path. With these optical sensitivities, the FEM calculated the optical-beam-path deflection at the SSM by multiplying the optical sensitivity of each component by its expected displacement.

The transmitter FEM consisted of 395 elements with 1860 degrees of freedom (Fig. 12). By computing the response of the FEM to the expected qualification test levels, we determined the anticipated structural stresses in the transmitter. The peak normal stress was predicted to be 142 MPa (20,650 psi), considerably less than the endurance limit for the 6Al-4V titanium alloy used, which has a yield stress of 882 MPa

(128,000 psi). This low stress level resulted from our minimizing the weight carried by the support struts. This design strategy provided a twofold benefit: it reduced the static and dynamic loads proportionately, and it raised the resonant frequencies in order to decouple the transmitter from the OMS vibrations.

The host spacecraft's momentum wheel, whose 6000-rpm rotation would generate vibrations at 100 Hz and its harmonic frequencies, would cause the primary operating disturbances (Table 3). To find the resulting transmitter line-of-sight jitter, we used the expected vibrational levels at the transmitter mounting location as inputs to the transmitter FEM (see the subsection "Development of a Test Plan" on p. 267). Table 4 shows the results of the analysis. In all cases the transmitter contribution to the system line-of-sight jitter is insignificant. This result is due in large part to the transmitter's high resonant frequencies. Data from a dynamic analysis of the FEM indicate that the first three modes of vibration occur at 281, 394, and 550 Hz. Modal measurements of the assembled transmitter show that its resonant frequencies are in close agreement with the FEM predictions.

Using the thermal model, we chose the size of the radiator to be just large enough to allow the lasers to be cooled to their minimum operating temperature of 10°C while the heaters are at their lowest power and the sun is shining on the radiator. Given this radiator size, the thermal model determined the corresponding heater power required with different solar illuminations and mounting-surface temperatures. Table 5 shows the results for the two cases that

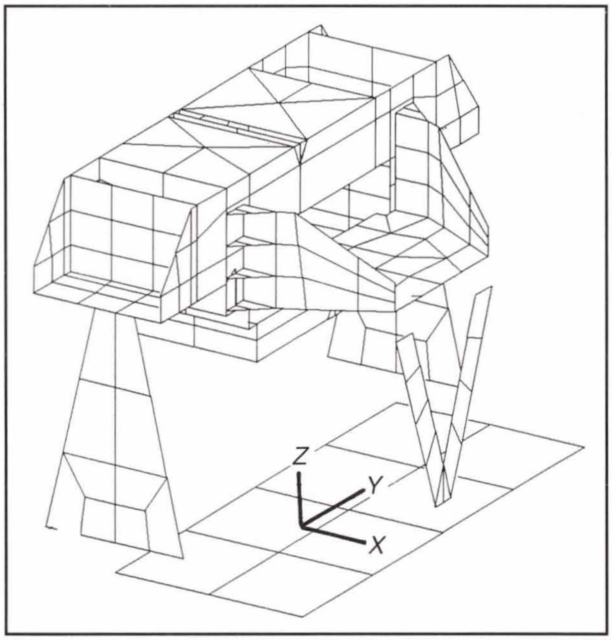

Fig. 12—Finite-element model of the transmitter, which allowed estimates of deflections and stresses to be made for various thermal and mechanical loadings. Optical path deflections were also found for the same conditions.

bound transmitter operation. Figure 13 depicts the temperature distribution for the minimum-power dissipation case. In both cases the expected translation of the beam at the SSM produced negligible throughput losses in the optical train of the OMS. For all operating scenarios, we expect that a heater power of less than 3.7 W can maintain a laser operating temperature of 30°C, and 1.5 W of heater power can maintain a survival temperature of –20°C.

We used computer ray-tracing optical analysis extensively during the transmitter development, particularly in the design of the collimator. This fast (f/1.1) lens group with a clear

Table 3. Expected Spacecraft Disturbances due to Momentum-Wheel Operation

Frequency (Hz)	*Acceleration (g) at OMS-Spacecraft Interface*		
	x	y	z
100	0.040	0.036	0.036
200	0.006	0.002	0.002
300	0.016	0.030	0.018

Table 4. Expected Transmitter Line-of-Sight Jitter due to Momentum-Wheel Operation

	Expected Jitter (μrad)	*Budgeted Jitter (μrad)*
Object space*		
Elevation	0.007	0.048
Azimuth	0.014	0.048
Radial	0.016	0.068

*Includes 40x telescope

aperture of 12 mm collimates the light emitted from the laser into a high-quality beam. All four of its elements, three lenses plus a flat corrector plate, were made from Schott G5 radiation-resistant glass. The collimator design minimized optical feedback, which can degrade laser performance, while it maintained high throughput.

We also used the optical-analysis model to estimate the quality of the transmitter beam's wavefront for different operating temperatures. Because a laser's operating temperature and current can change as the laser's efficiency degrades with age, the source assembly must be able to maintain a high-quality wavefront over a range of temperatures. We calculated those variations in the lens-assembly back focal length which resulted from (1) changes in the lens spacings due to the thermal growth of the housing, (2) changes in the curvatures of the lenses resulting from glass thermal growth, and (3) variations in the glass index of refraction with temperature. Similarly, from our knowledge of the geometry and materials used in the laser construction, we estimated the displacement of the laser emitter relative to its mounting flange. Calculations showed that careful selection of

Table 5. Characteristics of the Two Thermal Scenarios That Bound Transmitter Operation

	Case 1: Minimum Power Dissipation	*Case 2: Maximum Power Dissipation*
Laser temperature	10°C	30°C
Optomechanical Subsystem (OMS) bench temperature	14°C	0.5°C
Sun on transmitter radiator	Yes	No
Transmitter age	End of life	Beginning of life
Required power dissipation		
Heater	0.25 W	3.70 W
Electronics	0.71 W	0.49 W
Total	0.96 W	4.19 W
Beam translation at SSM	14 μm	30 μm
Signal loss due to beam truncation	0.02 dB	0.04 dB

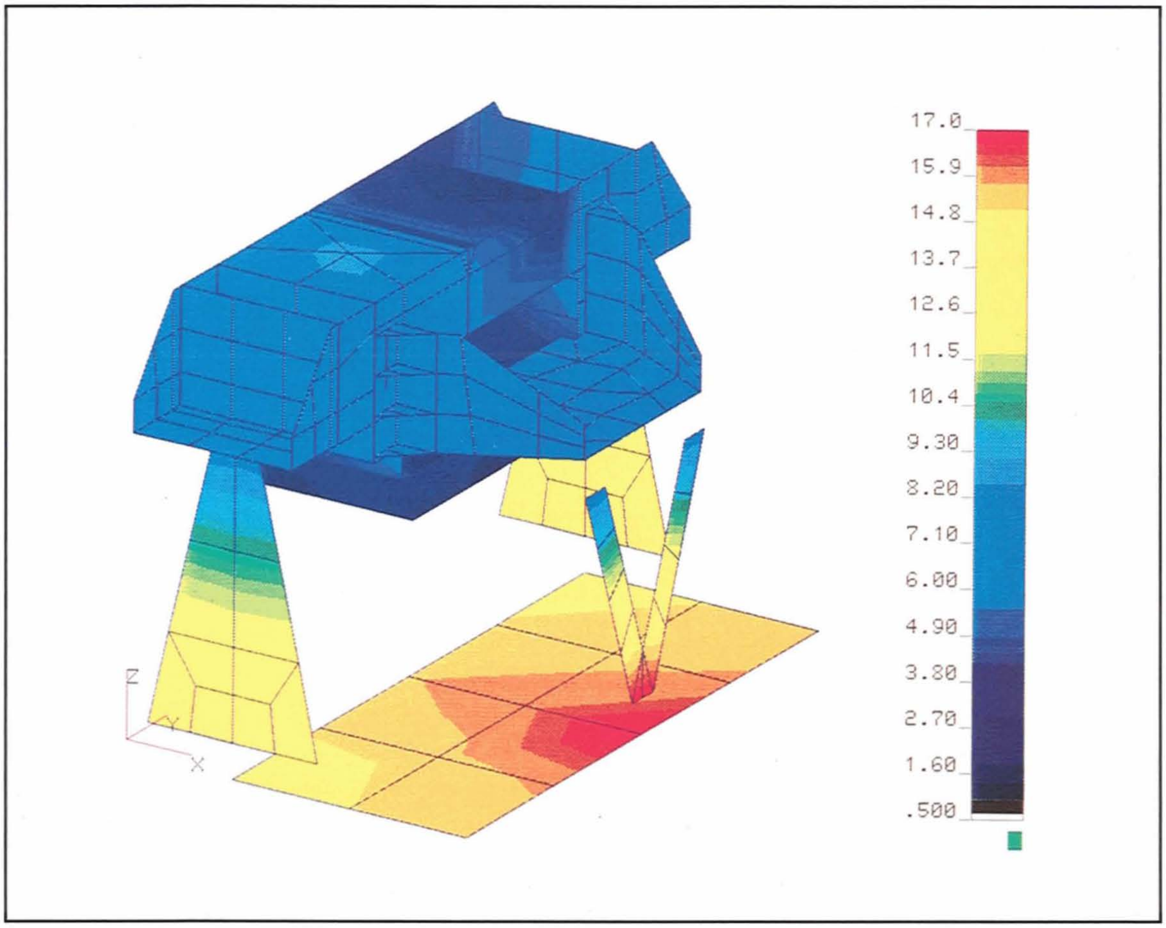

Fig. 13—Temperature profile of transmitter during minimum-power operation (case 1 of Table 5). The color profile represents the thermal gradients within the transmitter structure when the diode laser is operating at 10°C and the sun is illuminating the thermal radiator.

the material and length of spacers located between the collimator and laser could eliminate focus errors due to temperature changes (Table 6). Measurements, discussed in a later chapter, showed that this approach was successful.

Diagnostics System Description

The diagnostics system, which consists of the diagnostics module and the Transmitter Laser Controller (TLC), controls the laser operating point. At the start of a communications session, the SSM directs the transmitter beam into the diagnostics module. The TLC, which controls the laser bias current, temperature, and modulation current, uses the diagnostics-module sensor outputs to set the laser power, wavelength, and FSK tone spacing [11]. Once the adjustments are complete, the SSM directs the beam to the telescope for operation. Figure 14 is a block diagram of the diagnostics system.

The diagnostics system measures FSK tone spacing with a static, confocal Fabry-Perot interferometer (FPI) [12], which is a resonant optical cavity with multiple transmission passbands. The length of the FPI cavity determines the passband spacing, which was chosen to be about twice the width of the modulated laser spectrum. The cavity length and the reflectivity of the mirrors at either end of the cavity determine the width of the passbands and hence the resolution of the interferometer. To use the FPI as an optical spectrum analyzer, we sweep the laser spectrum through one of the passbands by ramping the laser bias current while the laser is being FSK-modulated. The output is detected by a photodetector consisting of a photodiode-amplifier hybrid at the output of the FPI. The

TLC interprets the spectrum and uses the results to adjust the modulation, thereby setting the FSK tone spacing to within 5 MHz of the nominal 220 MHz.

Accurate setting of the transmitter wavelength ensures that the heterodyne intermediate-frequency signal will fall within the bandwidth of the receiver. Such accuracy is achieved by a two-step process. First, a coarse measurement helps reduce the wavelength uncertainty to 1 Å, or 40 GHz. Then a fine wavelength setting reduces the uncertainty further to within 100 MHz of a known optical reference frequency.

The coarse-measurement procedure uses a thin-film, multilayer dielectric interference filter that has a wavelength-dependent transmission, as shown in Fig 15(a). Thus the transmitted power provides a measure of the beam wavelength. This design achieves the required wavelength resolution over the LITE transmit wavelength band of about 30 Å.

For a coarse wavelength measurement (lower left portion of Fig. 14), a laser beam is split into two parts, one of which passes through the interference filter. Each beam is then received by a separate photodetector similar to the one used by the tone-spacing subsystem. The photodetector that receives the unfiltered beam produces an accurate measurement of laser optical power. This measurement is also used to normalize the filtered-beam measurement. Be-

Table 6. Compensation for Thermal Focus Change in Source Assembly

Component	Displacement ($\mu m/10°C$)
Back focal length	0.457
Laser package	–0.533
Collimator mounting bracket	–0.013
Invar spacers	0.088
Total	0.000

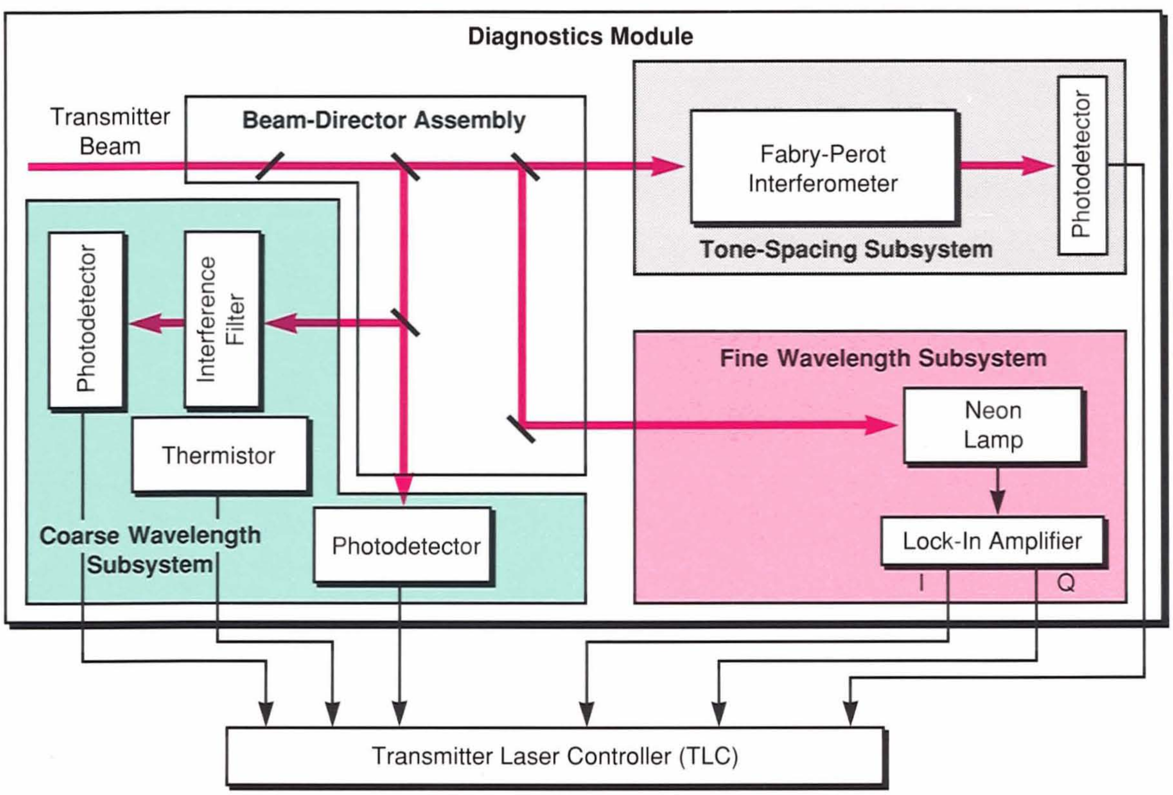

Fig. 14—Block diagram of diagnostics system.

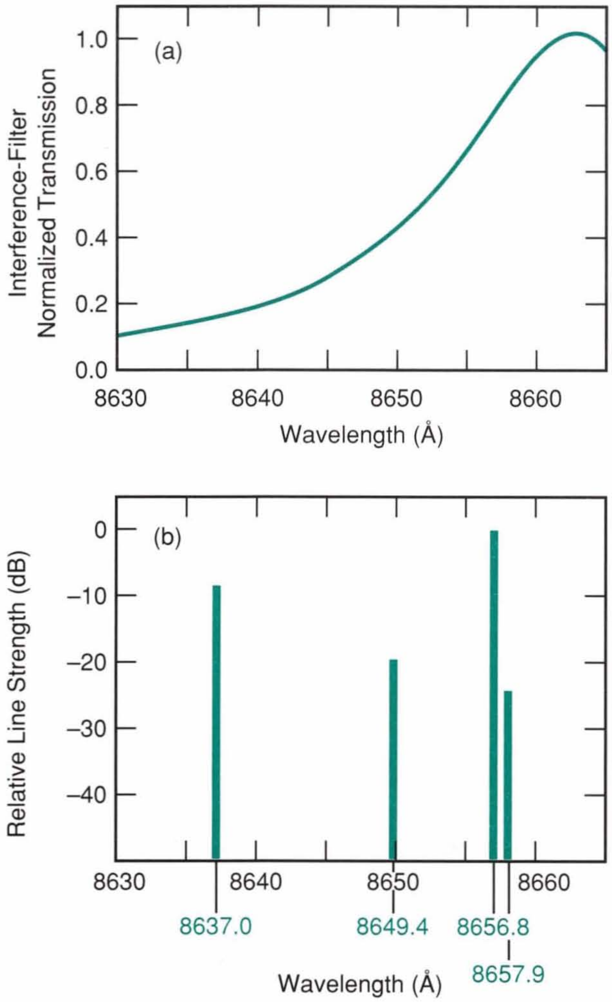

Fig. 15—(a) Normalized transmission characteristic of interference filter at 20°C and (b) relative spectroscopic strengths of the neon reference lines used in the diagnostics module. The line strength affects only the fine wavelength measurement SNR.

cause the transmission curve of the filter shifts with temperature by about 0.25 Å/°C, a thermistor mounted close to the filter measures the filter temperature so that a temperature correction can be applied to the wavelength estimate. From the two photodetector voltages, the known filter response, and the thermistor reading, the TLC can adjust the laser wavelength to within 1 Å.

To obtain a fine wavelength measurement, the diagnostics module makes use of a spectroscopic technique called optogalvanic detection [13]. In this technique, laser light resonant with an atomic transition of a gas in a discharge cell produces a change in the impedance of the cell. The resulting impedance difference is detected as a small change in the voltage drop across the cell. For the discharge cell, we used a low-cost, high-brightness neon lamp of the type used in instrument panels. Figure 15(b) shows that neon gas has four resonances within the lasers' operating range. The different heights correspond to signal strength and do not complicate the algorithm.

During a fine wavelength measurement, the TLC tunes the laser through one of the neon resonances. In order to extract the resulting small change in voltage drop from the lamp's large operating voltage, the TLC applies a 3-kHz modulation to the laser bias current to modulate the wavelength. A lock-in amplifier synchronously detects and demodulates the AC-coupled signal.

The section "Transmitter Laser Controller: Description of Algorithms" describes the algorithms for tone spacing and wavelength measurements in greater detail.

Diagnostics Module: Description of Hardware

We designed the diagnostics module to be a lightweight, space-qualifiable module with loose alignment tolerances, simple alignment procedures, and no thermal feedback-control requirements. The diagnostics-module housing, which consists of separate optics and electronics cavities as shown in Figs. 16 and 17, measures 50 mm × 133 mm × 203 mm and has a mass of 1.26 kg with covers. The optical cavity has components mounted directly to the interior walls in a way that avoids the use of L-brackets, thus simplifying the alignment process. The module has been designed to operate with possibly large variations in input-beam alignment (Table 7).

In order to reduce mechanical stress, the aluminum housing is kinematically supported by flexures that mount to the beryllium optical bench, which has a lower coefficient of thermal expansion than aluminum. These flexures combine with the light weight of the diagnostics module to create a first structural resonance of 375 Hz, which is well above the launch-spectrum peak. Since the bench temperature is well controlled and the diagnostics module dissipates only 1.1 W of electrical power, structural deformations from thermal stresses are minimal.

The electronics cavity contains the lock-in amplifier and power-distribution and filtering circuits. In critical areas, we thickened the aluminum frame around the electronics board to increase the radiation shielding.

A beam-director assembly determines the optical paths of the beams inside the diagnostics module (Fig. 14). The assembly consists of a series of 13-mm cube beam splitters bonded directly to an aluminum base. The first optical element in the assembly is a polarizing cube beam splitter that removes any polarization that is out of the plane of the optical bench. This polarization ensures that all subsequent measurements produce consistent results. The remaining beam splitters divide the beam into four parts for the different measurements.

We carefully selected the mounting locations of the components within the diagnostics module. For example, the beam that passes straight through the beam director goes to the FPI, which is most sensitive to beam angle and position. Thus beam-splitter tilts have a minimal effect on FPI performance. Also, to prevent the neon lamp from illuminating the photodetectors we located the lamp at the end of the series of beam splitters, far from the power monitor and coarse wavelength photodetectors. Finally, because the transmissivity of the interference filter de-

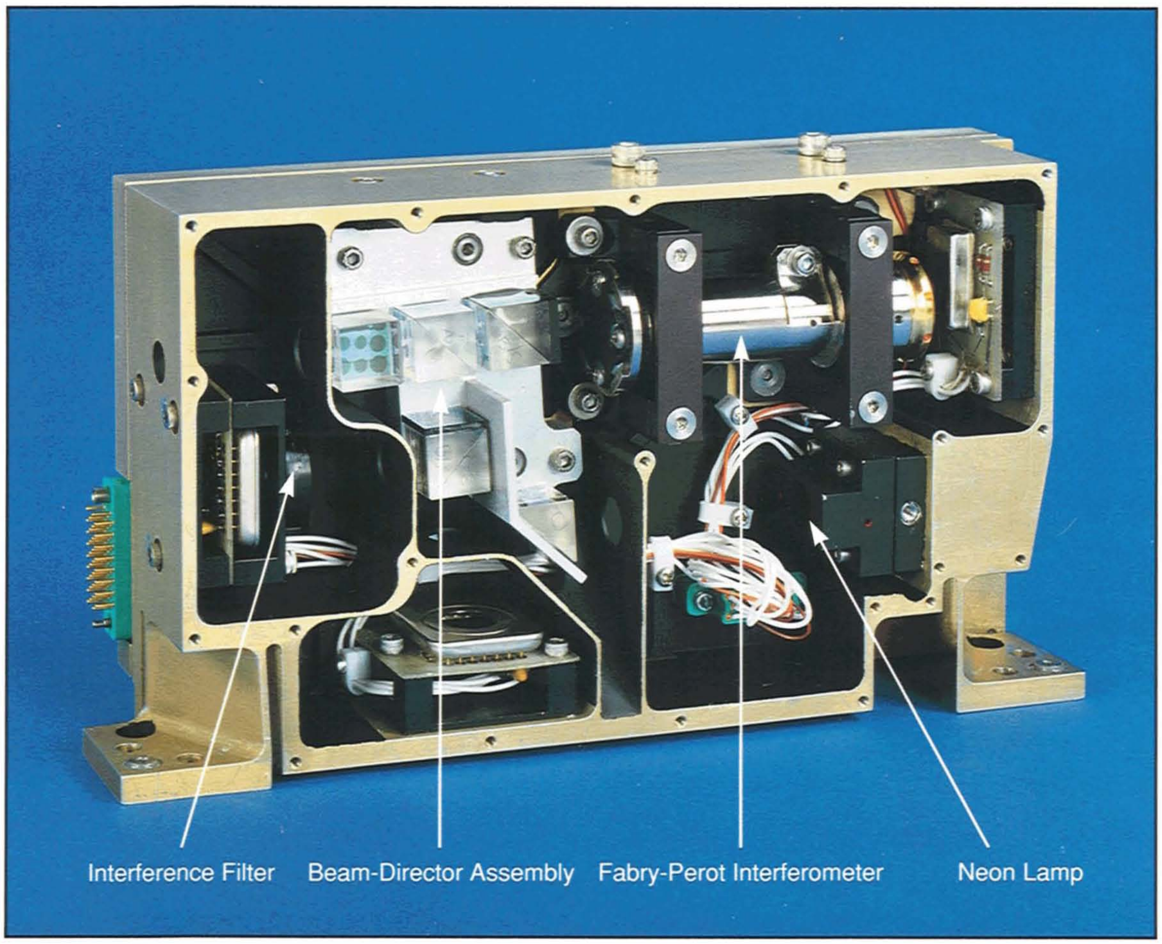

Fig. 16—Optics side of the diagnostics module, which contains all of the optical components required for accurately measuring the wavelength, power, and tone spacing of the transmitter beam. Note the internal baffles, which are used to control stray light reflections. The optics cavity cover is not shown.

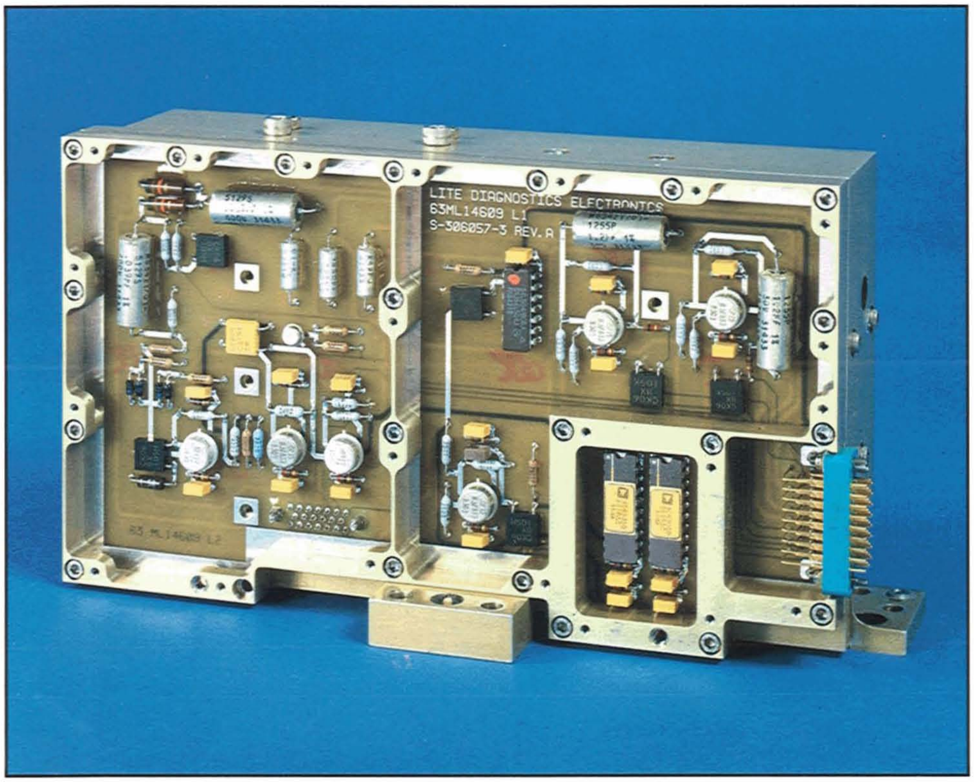

Fig. 17—Electronics side of the diagnostics module, shown without cover, where a lock-in amplifier and power-distribution and filtering circuits are located. Additional wall thickness provides needed radiation shielding for components susceptible to radiation damage.

pends on the angle of incidence of the beam, we arranged for one beam to follow a retroreflecting path through the beam director. Thus the angle of incidence at the interference filter was made insensitive to angular changes in the beam-director assembly.

We implemented various features to reduce optical feedback from the diagnostics module. For example, each optical element of the assembly is tilted with respect to the diagnostics-

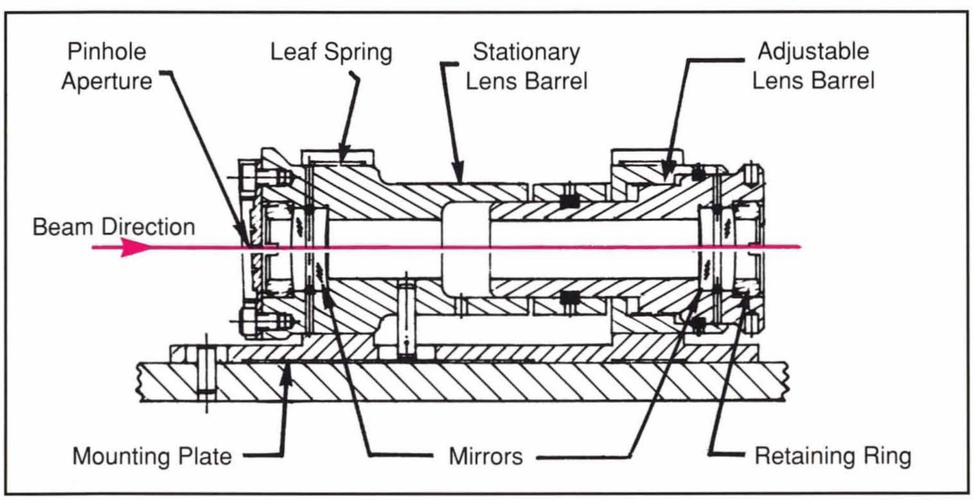

Fig. 18—Fabry-Perot interferometer (FPI), used to measure the optical spectrum of diode lasers.

Table 7. Range of Operating Parameters for Diagnostics Module

Parameter	*Minimum*	*Maximum*	*Units*
Temperature	9	30	°C
Input beam off center	–1	1	mm
Input beam tilt	–1	1	mrad
Input polarization	–1	1	degrees from parallel to optical bench
Supply voltage	–1	1	volts from nominal

module optical axis so that reflections do not return to the laser. For further feedback reduction, we inserted neutral-density filters and light shrouds at several locations, and we covered the inner surfaces of the housing with low-reflectivity black paint.

The FPI (Fig. 18) has an Invar lens barrel, which limits changes in mirror spacing to 0.6 μm for every 10°C temperature difference. Holding the mirror spacing constant over all operating temperatures keeps the spectral resolution constant. An adjustable lens cell in the barrel permits the mirrors, which are rugged versions of commercially available units, to be adjusted with respect to each other during assembly. To desensitize the alignment of the FPI to the incoming beam, a beam stop with a 1-mm-diameter aperture was placed at the entrance to the FPI.

Transmitter Laser Controller: Description of Algorithms

A set of iterative algorithms determines the operating parameters of the selected diode laser at the start of a session. The TLC initially sets the laser at the current and temperature for which the laser's wavelength is expected to match the neon reference. Usually the operating point from the last communications session is used. The TLC then executes the tone-spacing and wavelength algorithms to fine-tune the operating point.

As mentioned earlier, tone spacing can be deduced from the optical spectrum, which we can obtain by using the FPI as a spectrum analyzer. Scanning the FPI is accomplished by sweeping the laser bias current, and the resulting spectrum of the modulated laser is recorded.

The *tone-spacing algorithm* can be broken down logically into three sections:

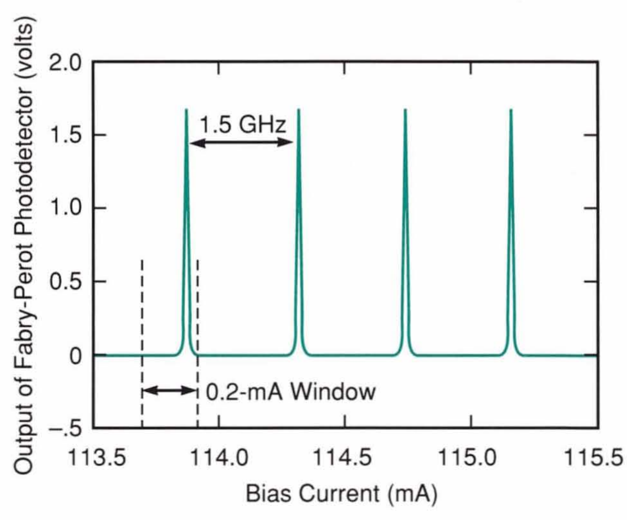

Fig. 19—Sweep of FPI on an unmodulated diode laser. Note the four equally spaced peaks. The distance in the frequency domain between the peaks is a constant (1.5 GHz) dictated by the length of the Fabry-Perot cavity. The ratio of the change in laser frequency to the corresponding change in bias current can be determined from this data. From the spectrum, we also identify the 0.2-mA window of current that is required to capture the first complete peak on an expanded scale. The remainder of the tone-spacing algorithm operates on this small window.

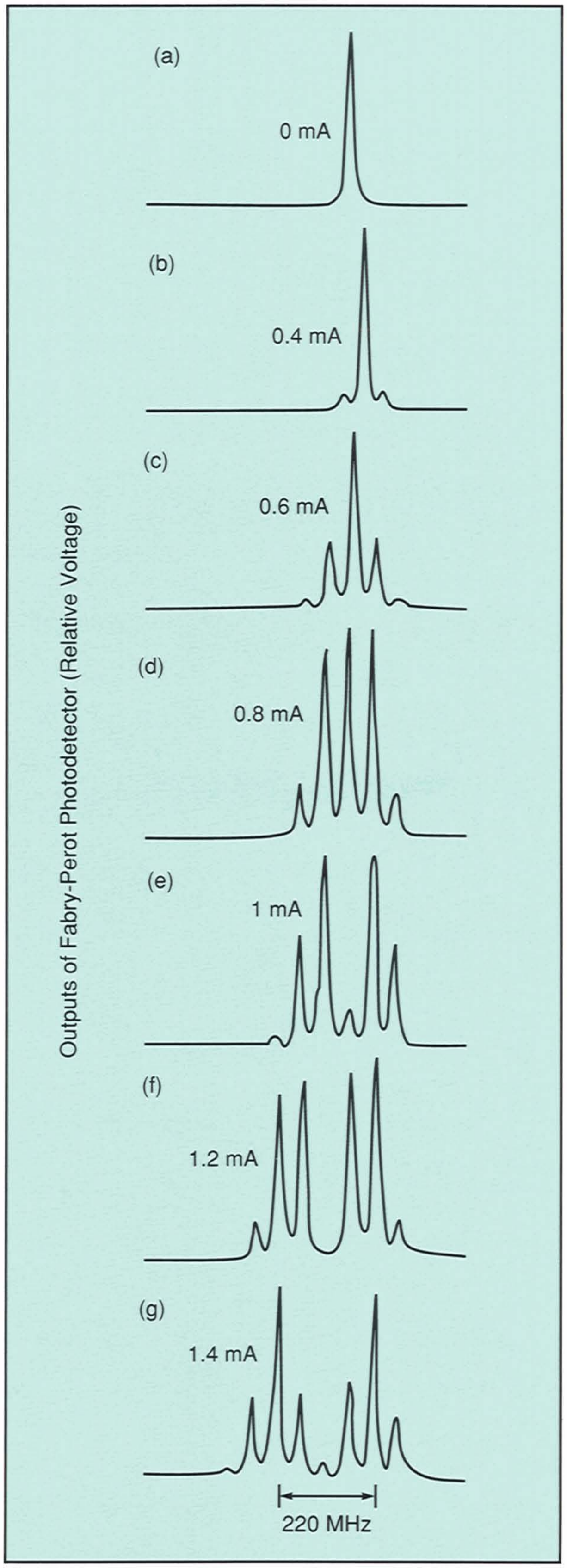

1. *Initialization.* To find the value of the laser DC tuning rate, the first sweep of the spectrum shown in Fig. 19 is taken on an unmodulated laser. That is, we find the change in bias current that is necessary to make the detected output of the FPI traverse two peaks of the unmodulated spectrum. The peaks, which are fixed by the geometry of the FPI cavity, are 1.5 GHz apart in our system. Thus the DC tuning rate can be calculated.

   From the unmodulated spectrum, we also identify a smaller spectral window that contains one complete peak. The remainder of the tone-spacing algorithm operates on this small window.
2. *Coarse tone spacing.* The TLC modulates the laser in a square-wave fashion at a 110-MHz rate between two tones that are a nominal 220 MHz apart. By modifying the amplitude of the modulation current, we can achieve different tone spacings. At each trial value of modulation current, a 1000-point spectrum is recorded in 2 sec by stepping the bias current. A simple eight-point moving average smooths the noisy waveform enough to allow the algorithm to determine the peaks unambiguously. Figure 20 shows the variation of measured spectra with modulation current.
3. *Fine tone spacing.* We can deduce the tone spacing by measuring the ratio between the second and first sidebands, as illustrated in Fig. 21. This ratio has been found to be a strong function of tone spacing. The ratio that corresponds to the desired tone spacing can be predicted.

As previously mentioned, the *wavelength algorithm* consists of two steps: first a narrowband interference filter helps to perform a coarse wavelength determination, then a neon atomic

Fig. 20—FPI output during sweeps of bias current on a diode laser. The sweeps (parts a through g) are for increasing amplitude values of modulation current. Note that the spacing between the largest peaks is close to 220 MHz at a modulation current of 1.4 mA (part g). With this coarse estimate of modulation current, the fine-tuning algorithm can commence.

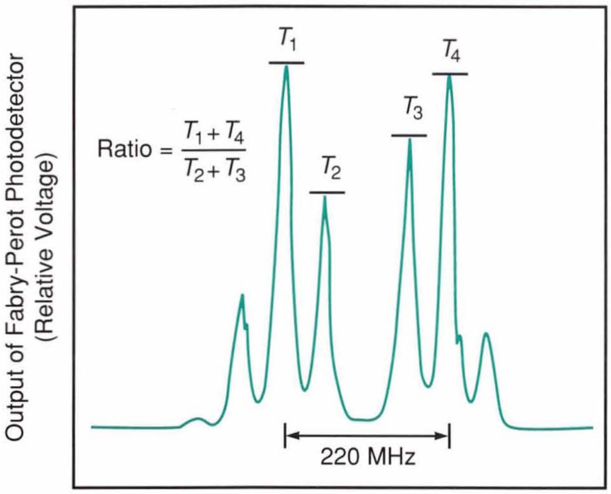

Fig. 21— FPI output during sweep of bias current on a modulated diode laser. The sweep was done near the tone-spacing frequency of 220 MHz. We can deduce the tone spacing by measuring the ratio between the second and first sidebands. The ratio varies steeply with tone spacing in the vicinity of 220-MHz spacing. A filtered optical spectrum is recorded for each trial modulation current and the current is then adjusted to produce the desired sideband ratio. When the ratio is within certain empirically determined bounds, the accuracy of the tone spacing will be within 5 MHz. The corresponding value of modulation current is saved for subsequent operations.

reference is used to conduct a fine wavelength measurement.

1. *Coarse wavelength tuning.* We can determine the transmission through the interference filter by computing the ratio from the output of the two photodetectors and then comparing the ratio to a temperature compensated filter-transmission curve.
2. *Fine wavelength tuning.* The TLC modulates the laser with a signal that alternates in a square-wave fashion between two tones 660 MHz apart at a rate of several kilohertz. The lock-in amplifier picks up the AC-coupled discharge voltage across the neon lamp and outputs inphase (I) and quadrature (Q) signals. The TLC digitizes the signals, which are used to find the center of the neon line.

Figure 22 shows the shape of the computed $I^2 + Q^2$ curve around the neon reference. In actual practice, the algorithm does not do a detailed plot of the $I^2 + Q^2$ curve but instead takes a series of samples (indicated by dots in Fig. 22) and looks for the presence of the neon reference line. Then, by using smaller steps, the algorithm searches for the zero crossing.

At the end of the algorithm, the laser optical power is checked again to verify that it is still within the operating specifications. If not, a power-correction routine that holds the wavelength approximately constant is activated, after which the wavelength is rechecked. If necessary, the wavelength-search and power-correction routines can be iterated until they converge to the reference wavelength and specified optical power.

After convergence, the laser operating parameters (DC bias current, modulation current, and temperature) are stored, and the system is ready for a communications session. In routine operation, the entire diagnostics algorithm takes a few minutes to run.

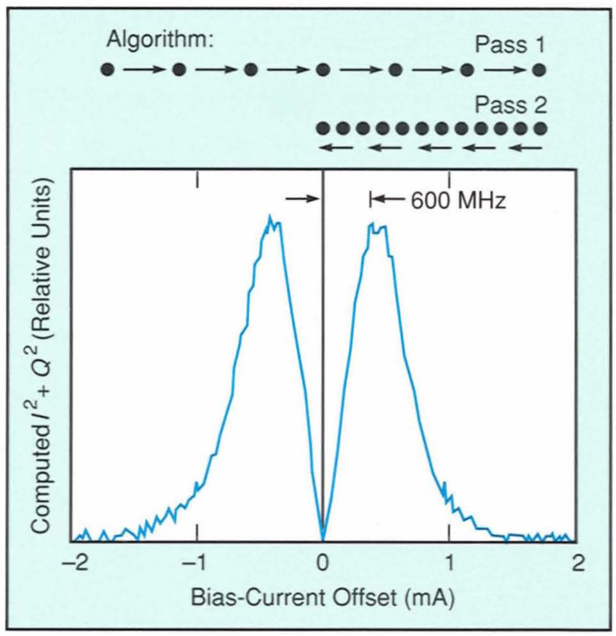

Fig. 22—Computed $I^2 + Q^2$ of the optical spectrum of an FSK-modulated laser. Analysis of the waveform allows the precise setting of laser wavelength. Samples (indicated by dots) are taken and for each point the quantity $I^2 + Q^2$ is computed. During the first pass, the algorithm finds the neon reference line and identifies which of the two signals (I or Q) is stronger. In the second pass, the algorithm looks for the zero crossing of the stronger signal (I or Q). Iteration continues until the frequency is within 100 MHz of the reference.

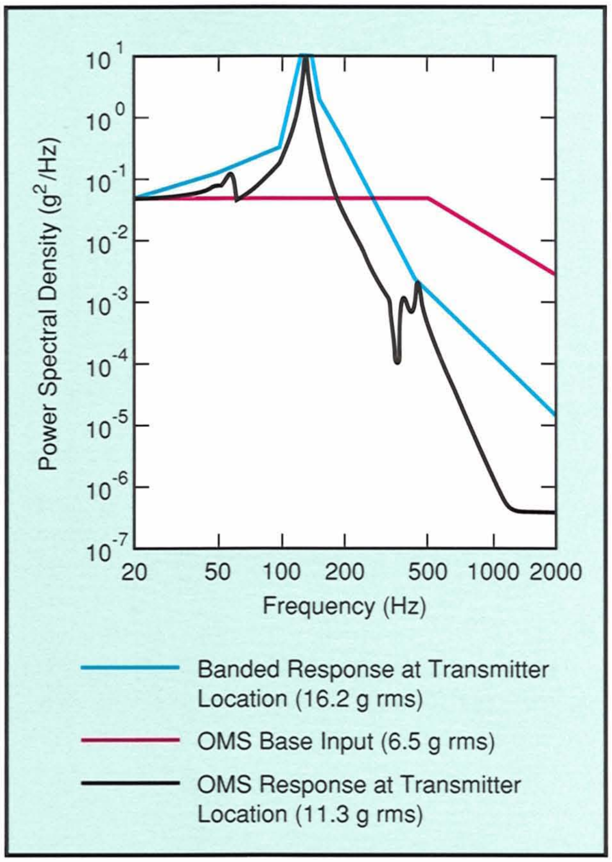

Fig. 23—Random-vibration power spectral density for the base of the Optomechanical Subsystem (OMS) and the transmitter mounting location. Note that high-frequency vibrations are effectively filtered out at the transmitter location. The banded response curve is used as the test level during qualification testing of the transmitter.

Qualification Testing

During the first several minutes of a launch, a satellite experiences an intense acoustic field. In addition, random and steady-state vibrations from the rocket motor are transmitted to the satellite via attachment points that secure the satellite to the rocket. After an initial orbit has been achieved, deployment of appendages such as antennas and solar-panel structures is initiated with the firing of pyrotechnic mechanisms that send shock waves throughout the satellite.

The spacecraft also undergoes large variations in temperature, particularly during transfer orbits in which the spacecraft moves in and out of the earth's shadow and the vehicle's orientation with respect to the sun varies. Until the solar-array panels are deployed, the available electrical power is limited to the satellite's battery capacity, which thereby restricts the use of electric heaters. Thus temperature swings within the spacecraft typically range from –30° to 60°C. Only minimum operation (such as the telemetry of critical data) is required of the satellite during the transfer orbit; however, the thermal stresses are potentially damaging.

Even after the final orbit is established and all systems are operational, the satellite must operate in a hostile environment. Typically, operating temperatures inside the structure vary from –5° to 50°C, a range in which the performance of many electrical circuits can vary.

In addition, phenomena such as cosmic radiation and micrometeorites can cause damage to critical electrical and optical components. Therefore, careful choice of components and materials is mandatory. A qualification test program, then, gives the spacecraft designer confidence that the package will survive the rigors of space.

Test Program

Qualifying a flight package such as the LITE package includes random-vibration testing, thermal cycling, and operation under various thermal conditions. In addition, those components which are prone to radiation damage must be subjected to various radiation dosages to determine the shielding requirements. The design must be verified by analysis to ensure adequate design factors of safety, safe failure modes, and tolerance to the expected radiation dosage. The tests and requirements apply to the complete assembled package in the integrated configuration.

For the LITE project, developing a new flight component was a multistep process. First we developed a design and a breadboard unit that satisfied the functional requirements. Once we had tested and verified this unit, we then constructed a qualification unit that faithfully implemented the critical breadboard design features and used flightworthy components, flight construction techniques, and quality-control procedures. We subjected this qualification unit to test levels more severe in magnitude and duration than the levels expected during flight in order to prove that the design was robust. The final step calls for the building of a flight unit identical in every respect to the qualification unit. This unit would be subjected to tests performed at levels and durations that are equal to those expected after integration into the host spacecraft. Without unduly stressing the unit, these acceptance tests would ensure that the workmanship, assembly procedures, and components used in the final unit are adequate for flight.

When we are considering a component that utilizes new technologies for inclusion in a design, we may subject the component by itself to a limited number of qualification tests to evaluate its suitability for spacecraft use. For the transmitter and diagnostics module, several critical components—the FPI, the diode laser, the collimator lens, and a complete source assembly—and a process to bond glass optical components to metallic substrates were tested before inclusion in the design.

Development of a Test Plan

The host-spacecraft program plan specified the expected conditions for prelaunch tests, launch, deployment, and operation. It also dictated the minimum allowable testing of the flight package. These test requirements were based on measurements taken during previous missions of similar satellites and on computer models of the actual structure and the expected loads. We made all acceptance-test levels more severe than the expected flight conditions to account for uncertainties in the measurements and modeling, and made the qualification levels still higher to ensure that the eventual flight package would pass all acceptance tests.

Qualification-level random-vibration tests were specified to be applied at the mounting feet of the OMS. The OMS mounting structure is a vibration-isolation system designed to minimize the effects of spacecraft vibrations [8]. It was important to remember that the dynamic response could be significantly different in magnitude and frequency content at various locations within the OMS. Thus, when a subassembly within the OMS was to be tested individually, the corresponding transfer function had to be taken into account. For example, Fig. 23 shows the power spectral density as a function of frequency for the base of the OMS and the expected power spectral density for the transmitter mounting location within the OMS. A detailed FEM of the complete OMS package helped generate the transfer functions. The banded response (Fig. 23) was used as the test level as a conservative way to account for uncertainties in the model.

The thermal tests require each subassembly, as well as the complete flight package, to function properly from 10°C below to 10°C above the operating range predicted by the computer thermal model. By using such a temperature range, we could demonstrate an adequate design margin. For demonstration of survival during the transfer orbits, the units were cycled to temperatures exceeding those expected during the orbit.

Transmitter Testing

Before the source assemblies were integrated into the transmitter, they underwent extensive characterization and testing. The testing was necessary to verify the quality of both the design and assembly procedures.

One of the most important performance criteria of the source assembly is the wavefront quality of the emitted beam. The wavefront quality determines the amount of spreading, or diffraction, of the beam as it travels to the receiver, which may be thousands of kilometers away. Beam aberrations such as defocus and spherical aberration govern wavefront quality. For a wavefront of high quality, the profile of the phase of the beam is flat. Thus wavefront quality can be measured by the deviation of the wavefront from a flat surface. Figure 24 shows the approximate relationship between the quality of a beam's wavefront and the power available at the receiver.

In order to verify the thermal focus-compensation design, we operated a source assembly over the 10°-to-30°C range, and recorded the wavefront quality at eight different tempera-

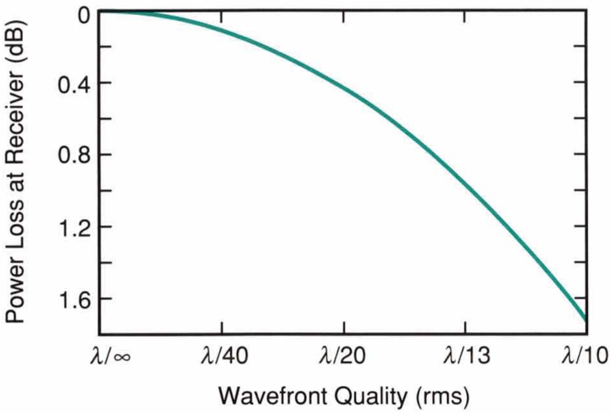

Fig. 24—Estimated power loss at receiver as a function of wavefront quality. The power loss at the receiver due to beam spreading is referenced to the ideal case in which there are no aberrations in the transmitted beam. The wavefront quality is measured by the rms deviation in the wavefront from a flat surface (λ = wavelength).

tures in the range. The results (Fig. 25) show a high-quality wavefront over the entire temperature range. The small focus error that varies with temperature is a result of the variations in the operating wavelength in combination with uncorrected chromatic aberration in the collimator. This error would not be present in our constant-wavelength operation.

We also performed thermal qualification testing on the unpowered source assembly to determine if it could withstand large temperature variations without suffering permanent deformations or displacements. The testing consisted of six cycles between –30° and 66°C over a three-day period. Operation of the heater during the transfer orbit made testing below –30°C unnecessary. The source assembly completed this testing without any change in operating characteristics.

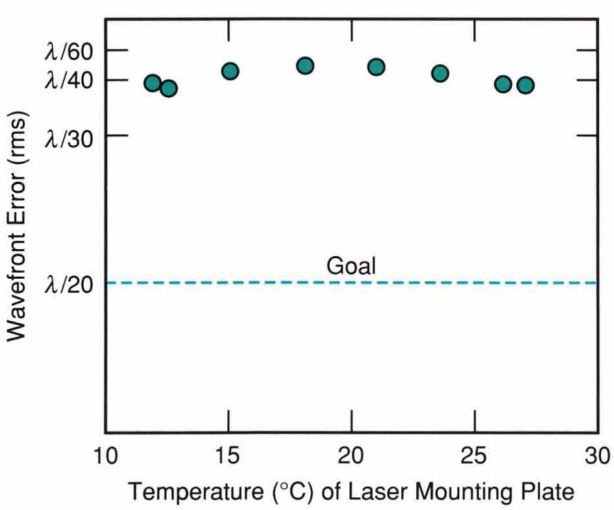

Fig. 25—Source-assembly thermal-compensation test results. Note that the laser wavefront's variation with temperature is small, and that the wavefront quality for the temperature range shown far exceeds the goal of λ/20 (rms).

Random vibrations can also cause optical aberrations by permanently displacing the laser, a lens element, or indeed the entire collimator. Thus it was important to subject the source assembly to random-vibration testing before building the complete transmitter so that the stability of the source assembly could be verified.

The random-vibration testing of the source assembly consisted of 2 min of vibration in each of three axes at increasing levels up to 35 g (rms). It is important to note that the expected vibration levels at the source-assembly locations during qualification of the OMS package were less than 11.5 g (rms). Subtracting the pre- and post-qualification wavefront profiles from each other revealed the changes in wavefront quality (Fig. 26). Within measurement error, we found that there were no changes in the wavefront quality or beam-pointing accuracy at the 15- and 22-g (rms) levels and only a small change at the 35-g (rms) level.

Once the robustness of the source assembly had been demonstrated, we fabricated four units and aligned them in the transmitter. Prior to qualification, the complete transmitter was characterized, with particular attention given to measurements of wavefront quality and beam-position accuracy.

Using an interferometer, we measured the wavefront quality of the transmitted beam from each of the integrated source assemblies in the same manner in which we had tested the individual source assemblies. Wavefront quality is expressed in terms of the deviation in the wavefront from a flat surface. The average wavefront quality of the four transmitted beams was $\lambda/26$ (rms). The $\lambda/26$ (rms) value, which includes the effects of prism and fold-mirror aberrations, was much better than our goal of

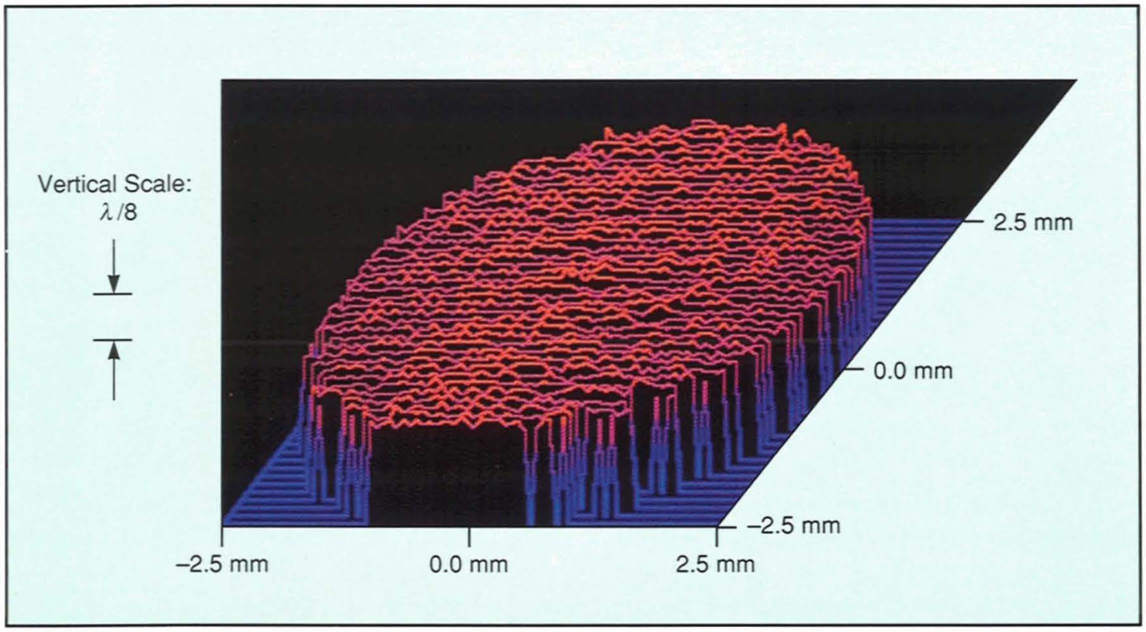

Fig. 26—Change in wavefront quality due to vibration testing at the 15-g (rms) level. The beam wavelength is 0.864 μm and the diameter is 5 mm.

$\lambda/20$ (rms). Furthermore, no individual beam's quality was worse than $\lambda/22$ (rms).

The vibration testing of the complete transmitter consisted of 2 min of random vibration in each of three axes at levels up to 16.2 g (rms). The thermal testing included the same six cycles of temperature (–30° to 66°C) that were used to test the source assembly. The average of the wavefront qualities remained unchanged by the random-vibration testing. The thermal qualification tests changed the wavefront quality by a small amount, from $\lambda/26$ (rms) to $\lambda/23$ (rms).

To determine the expected truncation losses within the OMS telescope, we measured the changes in the transmitter beam positions as a result of the qualification testing. After all qualification testing was completed, the average beam position had moved by less than 30 μm, which corresponds to a truncation loss of less than 0.04 dB.

In addition to tests of wavefront quality and beam-position accuracy, we measured the optical power of the laser outputs and found that each beam's power was between 26 and 26.5 mW. Thus the loss within the transmitter was less than the goal of 0.8 dB.

The final test of the transmitter was a demonstration of the communications capability of the unit. In a laboratory environment, random data were sent to a modulator which, in turn, sent the FSK waveform to the operating laser at a rate of 220 Mb/sec. The modulated beam was sent to a balanced receiver that demodulated the signal and recovered the transmitted data. This testing was the first demonstration of high-data-rate communications with a flight-qualified transmitter.

Diagnostics-Module Testing

Before including the key components in the final diagnostics-module design, we tested the components individually. The circuit board of the lock-in amplifier underwent thermal cycling, and a prototype of the FPI, the photodetector assemblies, and a neon lamp were subjected to both thermal cycling and random-vibration testing. The thermal-cycle temperatures used were the same as those required to qualify the complete diagnostics module; the vibration levels were at least as high as those required for the complete diagnostics module. We observed no failures or significant parameter changes in the tests.

In addition, the complete diagnostics-module

Table 8. Neon-Lamp SNR Budget for Acceptable Performance of the Fine Wavelength Algorithm

Average measured SNR of neon lamp	28.8 dB
Worst-case loss from beam misalignment	–5.4
Test-system power correction	8
Lock-in bandwidth reduction	10
Expected radiation darkening	–2
Weakest neon line	–23
Worst-case SNR of neon lamp	16.4 dB
Requirement for 100-MHz accuracy	13 dB
Margin available for implementation losses	3.4 dB

assembly underwent two types of environmental stresses. A thermal-cycle test subjected the unpowered diagnostics module to temperatures of –40° to 66°C for six cycles at a maximum rate of change of 20°C/h. We also subjected the diagnostics module to random vibration in three orthogonal directions at accelerations of 10.2 to 15.4 g (rms).

Before and after subjecting the diagnostics module to random vibration and thermal cycling, we functionally tested it over a range of operating conditions (Table 7). The tests were performed in a dedicated test system in which the diagnostics module was mounted in a temperature-controlled box. The diagnostics-module housing was located with respect to a reference axis established outside the box. During the tests, a laser whose alignment varied in angle and position with respect to the external reference axis was directed into the diagnostics module, and the resulting noise, offset, and signal voltages from the lock-in amplifier and all of the photodetectors were recorded. Independent power- and wavelength-measuring instruments checked the diagnostics-module measurements while a microprocessor-based test controller collected and interpreted the data.

Throughout the full range of operating parameters, the diagnostics-module test system correctly estimated laser wavelengths from the interference-filter-subsystem signals, with errors of less than 1 Å. The SNR of the neon lamp was also measured over the full range of operating parameters as an indirect measure of the quality of the diagnostics-module fine wavelength measurements. From previously collected data, we knew that an accuracy of 100 MHz in optical frequency was achievable if the SNR at the input to the lock-in amplifier was at least 13 dB. Table 8 shows that even under worst-case conditions, there is still adequate margin for achieving this accuracy.

To qualify the tone-spacing subsystem, we measured the frequency linewidth of an unmodulated laser, including the effects of transmission through the FPI. The resulting full-width-at-half-maximum (FWHM) values gave a measure of the resolution of the tone-spacing unit. Prior to environmental-stress testing, we measured the FPI FWHM over the full range of parameters, and found that the average value was 23.5 MHz. Remember that variations of FWHM will affect the accuracy of tone-spacing measurements. A calculated budget of 7 MHz for FWHM variability ensures a workable tone-spacing accuracy of 5 MHz. We found that the FWHM variations before and after environmental-stress testing were well below 7 MHz, and that the post-stress average FWHM was 24.7 MHz.

Summary

We have designed, built, and tested a transmitter system for free-space, FSK heterodyne optical communications, and the key hardware of the system has been qualified for space applications. The hardware consists of two compact, lightweight modules: a transmitter and a companion diagnostics module. Both devices passed a rigorous program of qualification tests. In addition, transmitter operation was demonstrated in a laboratory communications link that operated at 220 Mb/sec. The hardware is now available for incorporation into an engineering model of a satellite laser communications package.

The transmitter provides 26 mW of optical power from a single GaAlAs diode laser operating near 0.8 μm. The laser output has the necessary frequency stability and spectral purity for heterodyne communications. In addition, beam divergence is minimal—the measured deviation in the wavefront of each beam is less than $\lambda/22$ (rms).

The diagnostics module is capable of measuring laser power, optical frequency, and FSK tone spacing to better than the accuracies that heterodyne optical communications requires. The transmitter laser controller uses these measurements for the automatic setting of laser power to within 1 mW, optical frequency to within 100 MHz of a known reference, and FSK tone spacing to within 5 MHz of a nominal 220 MHz.

The successful thermal and random-vibration testing of the qualification transmitter and diagnostics module indicates that flight units of the same design would meet our requirements in a space environment. The space qualification of our transmitter is a milestone: it is the first laser transmitter proved flightworthy for high-data-rate optical communications in space.

Acknowledgments

The authors acknowledge the contributions of V. Jayaraman, G. Loney, D. Welford, and M. Richardson to the design of the transmitter system. The authors also thank V.W.S. Chan and D. Boroson for their technical direction as well as D. Kelly and C. Marangoudakis for their technical assistance. This work was sponsored by the Department of the Air Force.

References

1. C.-C. Chen and J.A. Schwartz, "Space Station-Based Deep-Space Optical Communication Experiments," *Proc. SPIE* **885,** 18 (1988).
2. M. Ross, "The History of Space Laser Communications," *Proc. SPIE* **885,** 2 (1988).
3. V.W.S. Chan and J.E. Kaufmann, "Coherent Optical Intersatellite Crosslink Systems," *Proc. SPIE* **988,** 325 (1988).
4. J.T. Verdeyen, *Laser Electronics* (Prentice Hall, Englewood Cliffs, N.J., 1981).
5. D. Begley and B. Boscha, "Laser Diodes Conquer the Challenges of Space Communications," *Photonics Spectra*, 147 (Apr. 1989).
6. J.L. VanHove and C. Noeldeke, "In-Orbit Demonstration of Optical IOL/ISL—The SILEX Project," *Intl. J. Satellite Comm.* **6,** 119 (1988).
7. V.W.S. Chan, "Intersatellite Optical Heterodyne Communication Systems," *Lincoln Laboratory J.* **1,** 169 (1988).

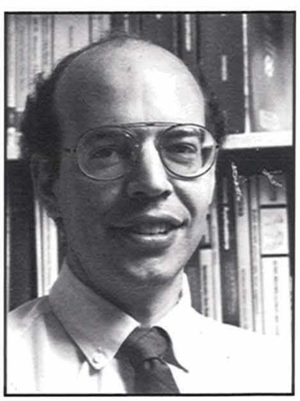

DAVID F. McDONOUGH received a B.S. and an M.S. in electrical engineering from MIT. Upon graduation, he helped develop the Multiple Mirror Telescope at the University of Arizona and worked for various West Coast companies in the electro-optics field. Dave joined Lincoln Laboratory in 1986; he is currently a staff member in the Optical Communications Technology Group, where he specializes in electro-optical sensors and optical measurement systems. He has been an active distance runner since 1969.

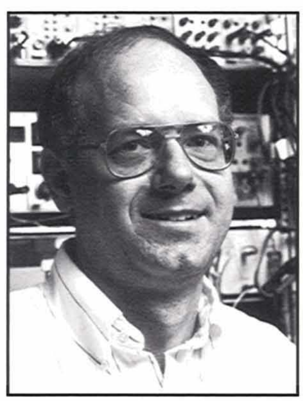

JOHN A. TAYLOR is a staff member in the Optical Communications Technology Group, where he has designed and developed electro-optical hardware for the Laser Intersatellite Transmission Experiment. Before joining Lincoln Laboratory seven years ago, John worked on low-noise receivers for the Five College Radio Astronomy Observatory. He graduated with a B.S. in physics from Davidson College, and an M.S. in physics and a Ph.D. in electrical engineering from the University of Massachusetts at Amherst.

8. R.S. Bondurant, S.B. Alexander, V.W.S. Chan, A.A. Colao, J.E. Kaufmann, E. Lee, A.N. Madiwale, P.F. Martin, A.D. Pillsbury, and E.A. Swanson, "An Opto-Mechanical Subsystem for Space Based Coherent Optical Communication," *Proc. SPIE* **996,** 92 (1988).
9. A.D. Pillsbury and J.A. Taylor, "Optomechanical Design of a Space-Based Diode-Laser Transmitter Assembly," *Proc. SPIE* **1044,** 112 (1990).
10. J.A. Taylor, A.D. Pillsbury, M.F. Richardson, and D. Welford, "Diode-Laser Transmitter Development for Space-Based Heterodyne Communication," *Technical Report 845*, Lincoln Laboratory (22 Mar. 1989), DTIC #AD-A208212.
11. V. Jayaraman, E.S. Kintzer, J.G. Garcia, and A.D. Pillsbury, "Design and Performance of an On-Satellite Laser Diagnostics System for a Free Space Optical Heterodyne Frequency-Shift-Keyed Communication System," *Proc. SPIE* **996,** 84 (1988).
12. R.S. Longhurst, *Geometrical and Physical Optics*, 3rd edition (Longman, New York, 1973), pp. 195–196.
13. S. Yamaguchi and M. Suzuki, "Simultaneous Stabilization of the Frequency and Power of an AlGaAs Semiconductor Laser by Use of the Optogalvanic Effect of Krypton," *IEEE J. Quantum Electron.* **QE-19,** 1514 (1983).

ALLEN D. PILLSBURY is a staff member in the Mechanical Engineering Group at Lincoln Laboratory, where he concentrates on the design of optical packages for use in space-based laser communications. Before joining Lincoln Laboratory in 1983 he worked at the Lawrence Livermore National Laboratory on the design of a large diamond-turning machine. Al received B.S.M.E. and M.E.M.E. degrees in 1979 and 1980, respectively, from the Rensselaer Polytechnic Institute.

DOMINIQUE P. VERLY was born in Liège, Belgium. She received an Ingénieur Electronicien degree from the University of Liège in 1975. Before coming to Lincoln Laboratory in 1980, Dominique worked at Amdahl Corporation in Sunnyvale, California, where she designed high-speed digital test systems. At Lincoln's Satellite Communications Electronics Group, she has developed architectures for signal processors, and designed signal processing VLSI devices and the hardware and software for real-time control systems.

Since 1988, Dominique has been a member of the LITE project, where she has participated in the design of the controller that implements the algorithms described in this article. She is currently designing the controller in charge of the moving elements in the optical train of the transmitter.

EMILY S. KINTZER is a staff member in the Optical Communications Technology Group. She received a B.A. in physics and mathematics from Wellesley College, a M.S. in physics from the University of Michigan, and a Ph.D. in applied physics from Stanford University. Emily joined Lincoln Laboratory after a postdoctoral fellowship at the Max Planck Institute for Biophysical Chemistry in Göttingen, W. Germany, where she worked on picosecond dye laser systems. Emily is currently working on the development of high-power coherent semiconductor laser sources for free-space optical communications.

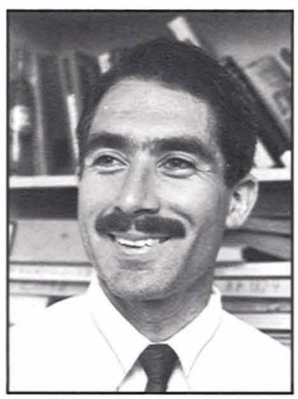

JAMES G. GARCIA is a staff member in the Mechanical Engineering Group, where he specializes in opto-mechanical design. Before joining Lincoln Laboratory five years ago, Jim worked for the Perkin-Elmer Corporation on various projects, including the Hubble Space Telescope. He received a B.S. and an M.S. in mechanical engineering from MIT.